Nanomaterials

PART-I: FABRICATION TECHNIQUES

Nanofabrication via different techniques: Sputtering, Sol–Gel Processing, Co-Precipitation, Electrodeposition, Solid State Synthesis, Chemical Vapor Deposition (CVD), Physical vapor Deposition (PVD).

PART-II: CHARACTERIZATION OF NANOMATERIALS

X-Ray Diffraction (XRD), Electron beam microscopy (SEM along with EDAX), Transmission Electron Microscopy (TEM), Atomic Force Microscopy (Scanning Tunneling Microscopy), Vibratory Sample Magnetometer (VSM), Ellipsometry, Fourier Transform Infrared spectroscopy (FTIR), 4-Probe Methods.

X-ray Diffraction

The atomic planes of a crystal cause an incident beam of x-rays to diffract and the diffracted rays interfere with one another as they leave the crystal. The phenomenon is called X-ray diffraction.

X-Ray Diffraction (XRD) is very useful technique. It:

1) Measure the average spacing between layers or rows of atoms
2) Determine the orientation of a single crystal or grain
3) Find the crystal structure of an unknown material
4) Measure the size, shape and internal stress of small crystalline regions

Basic Features of Typical XRD Experiment

1) Production of x-rays beam
2) Sample causing the diffraction of beams
3) Detection of the diffracted beams
4) Interpretation of data obtained

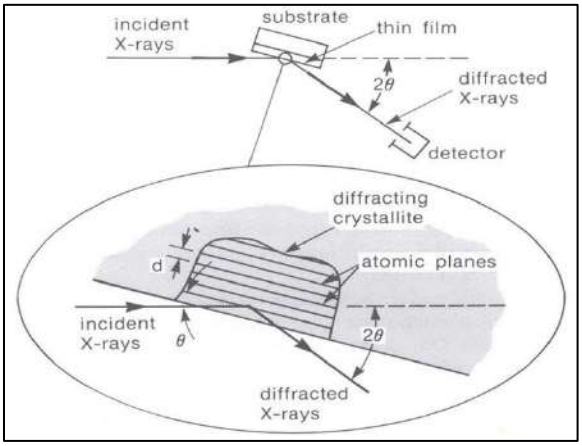

In a crystalline material, x-rays diffracted by atomic periodic planes will be interfere constructively in certain directions by satisfying Bragg's law.

Bragg's Law: Suppose two x-ray waves (X-ray 1 and X-ray 2) are incident on a periodic lattice of crystalline material and the waves are diffracted from the atomic periodic planes. The

periodic lattice acts as a diffraction grating for incident x-ray beams. Two important geometrical facts are:

- The incident beam, the normal to the reflecting plane, and the diffracted beam are always coplanar.
- The angle between the diffracted beam and the transmitted beam is always 2θ. This is known as the diffraction angle, and it is this angle, rather than θ, which is usually measured experimentally.

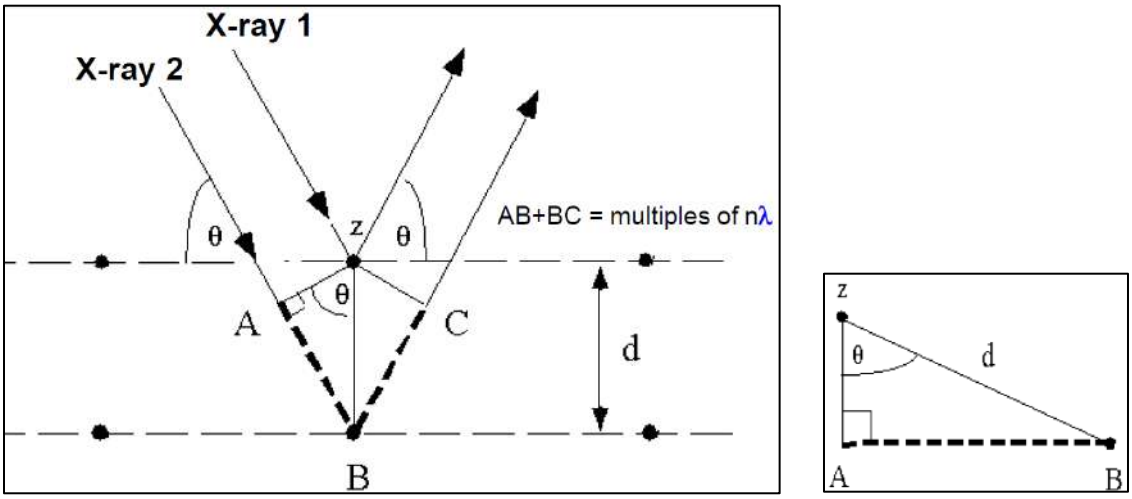

From the figure, constructive interference for the diffracted waves occurs only when n λ = AB + BC and AB=BC. So n λ = 2AB. From figure, Sin θ = AB/d that is AB = d sin θ and hence

$$n\lambda = 2d\sin\theta \qquad \text{(or for n=1, } \lambda = 2d_{hkl}\sin\theta_{hkl}\text{)}$$

Where d is the distance between lattice planes in a crystal, λ is the wavelength of the incident x-ray beam, n is an integer called order of diffraction and θ is the angle of incidence with lattice plane. This is an example of x-ray wave interference and commonly known as x-ray diffraction (XRD). Bragg's law showed that **diffraction occurs only when the wavelength of the incident wave is of the same order of magnitude as d; the distance between lattice planes in the crystal i.e. λ ≤ 2d.**

XRD was direct evidence for the periodic atomic structure of crystals. This law was presented by the Braggs and they were awarded the Nobel Prize in physics in 1915 for their work in determining crystal structures beginning with NaCl, ZnS and diamond. Although Bragg's law

was used to explain the interference pattern of x-rays scattered by crystals, diffraction has been developed to study the structure of all states of matter with any beam, e.g., ions, electrons, neutrons, and protons, with a wavelength similar to the distance between the atomic or molecular structures of interest.

Diffraction methods:

Hence diffraction occurs only whenever the Bragg law, $\lambda = 2d \sin\theta$, is satisfied. Some ways of satisfying the Bragg law has been devised. In these devices, XRD takes place by continuously varying either λ or θ during the experiment. The ways in which these quantities are varied distinguish the three main diffraction methods:

Method	**λ**	**θ**
Laue Method	Variable	Fixed
Rotating Crystal Method	Fixed	Variable (in parts)
Powder Method	Fixed	Variable

Sample Preparation

A sample made up of some hundreds of crystals (i.e. a powdered sample). Sample may be made of single crystal, poly, and amorphous materials. Sample may be powder, film and pallet forms. In powder, particle size ranges from 0.1µm to 40 µm. When particle size is of few µm less diffraction occurs but sharp peaks are obtained and when particle size is large, more diffraction occurs with peak broadening.

Applications of XRD

XRD is a nondestructive technique and it is used:

- To identify crystalline phases and orientation
- To determine structural properties: Lattice parameters (10-4Å), strain, grain size, expitaxy, phase composition, preferred orientation (Laue) order-disorder transformation, thermal expansion

- To measure thickness of thin films and multi-layers
- To determine atomic arrangement
- Detection limits: ~3% in a two phase mixture; can be ~0.1% with synchrotron radiation
- Phase Identification
- XRD Study pattern changes with temperature, Electric Field, Pressure and Deformation of the sample

The x-rays produced by transitions from the n=2 to n=1 levels are called K_α x-rays, and those for the n=3 to n=1 transitions are called K_β x-rays. Transitions to n=2 or L-shell are designated as L x-rays (n=3→2 is Lα, n=4→2 is L_β etc).

X-rays produced by any x-ray generator are heterogeneous in energy. The energy spectrum shows a continuous distribution of energies of the bremsstrahlung photons, on which the discrete lines of characteristic radiation are superimposed. Some of the commonly used x-ray K wavelengths (Å) are given in the table below:

Element	**Kα (av.) (Å)**	**$K\alpha_1$ (Å)**	**$K\alpha_2$ (Å)**	**$K\beta_1$(Å)**
Cr	2.29100	2.28970	2.29361	2.08487
Fe	1.93736	1.93604	1.93998	1.75661
Co	1.79026	1.78897	1.79285	1.62079
Cu	1.54184	1.54056	1.54439	1.39222
Mo	0.71073	0.70930	0.71359	0.63229

Intensity of the diffracted x-rays are detected by a detector (Fluorescent screens, Photographic film or Ionization devices) only if the sample, source and detector are placed properly after determining focusing circle at the circle of diffraction as shown in figure.

Crystal Structure Determination

- Obtain XRD pattern
- Measure d-spacings using the following formulae

System	d_{hkl}
Cubic	$\left[\frac{1}{a^2}(h^2 + k^2 + l^2)\right]^{-1/2}$
Tetragonal	$\left[\frac{h^2 + k^2}{a^2} + \frac{l^2}{c^2}\right]^{-1/2}$
Orthorhombic	$\left[\frac{h^2}{a^2} + \frac{k^2}{b^2} + \frac{l^2}{c^2}\right]^{-1/2}$
Hexagonal	$\left[\frac{4}{3a^2}(h^2 + hk + k^2) + \frac{l^2}{c^2}\right]^{-1/2}$
Rhombohedral	$\left[\frac{1}{a^2}\frac{(h^2 + k^2 + l^2)\sin^2\alpha + 2(hk + kl + lh)(\cos^2\alpha - \cos\alpha)}{1 - 2\cos^3\alpha + 3\cos^2\alpha}\right]^{-1/2}$
Monoclinic	$\left[\frac{\frac{h^2}{a^2} + \frac{l^2}{c^2} - \frac{2hl\cos\beta}{ac}}{\sin^2\beta} + \frac{k^2}{b^2}\right]^{-1/2}$
Triclinic	$\left[\frac{\frac{h^2}{a^2}\sin^2\alpha + \frac{k^2}{b^2}\sin^2\beta + \frac{l^2}{c^2}\sin^2\gamma + \frac{2hk}{ab}(\cos\alpha\cos\beta - \cos\gamma) + \frac{2kl}{bc}(\cos\beta\cos\gamma - \cos\alpha) + \frac{2lh}{ca}(\cos\gamma\cos\alpha - \cos\beta)}{1 - \cos^2\alpha - \cos^2\beta - \cos^2\gamma + 2\cos\alpha\cos\beta\cos\gamma}\right]^{-1/2}$

l

- Obtain integrated intensities
- Compare data with known standards in the JCPDS file, which are for random orientations (there are more than 50,000 JCPDS cards of inorganic materials).

Systematic absences

Symmetry element		Affected reflection	Condition for reflection to be present
Primitive lattice	P	*hkl*	none
Body-centered lattice	I	*hkl*	$h + k + l$ = even
Face-centered lattice	A	*hkl*	$k + l$ = even
	B	*hkl*	$h + l$ = even
	C	*hkl*	$h + k$ = even
Face-centered lattice	F	*hkl*	*h k l* all odd or even
twofold screw, 2_1 along	*a*	*h*00	*h* = *even*
fourfold screw, 4_2 along	*a*	*h*00	*h* = *even*
sixfold screw, 6_3 along	*c*	00*l*	*l* divisible by 3
threefold screw, 3_1, 3_2 along	*c*	00*l*	*l* divisible by 3
sixfold screw, 6_2, 6_4 along	*a*	*h*00	*h* divisible by 4
fourfold screw, 4_1, 4_3 along	*a*	*h*00	*h* divisible by 4
sixfold screw, 6_1, 6_5 along	*c*	00*l*	*l* divisible by 6
Glide plane perpendicular to	*b*		
Translation *a*/2 (*a* glide)		*h*0*l*	*h* = even
Translation *c*/2 (*c* glide)		*h*0*l*	*l* = even
b/2 + *c*/2 (*n* glide)		*h*0*l*	$h + l$ = even
b/4 + *c*/4 (*d* glide)		*h*0*l*	h + l divisible by 4

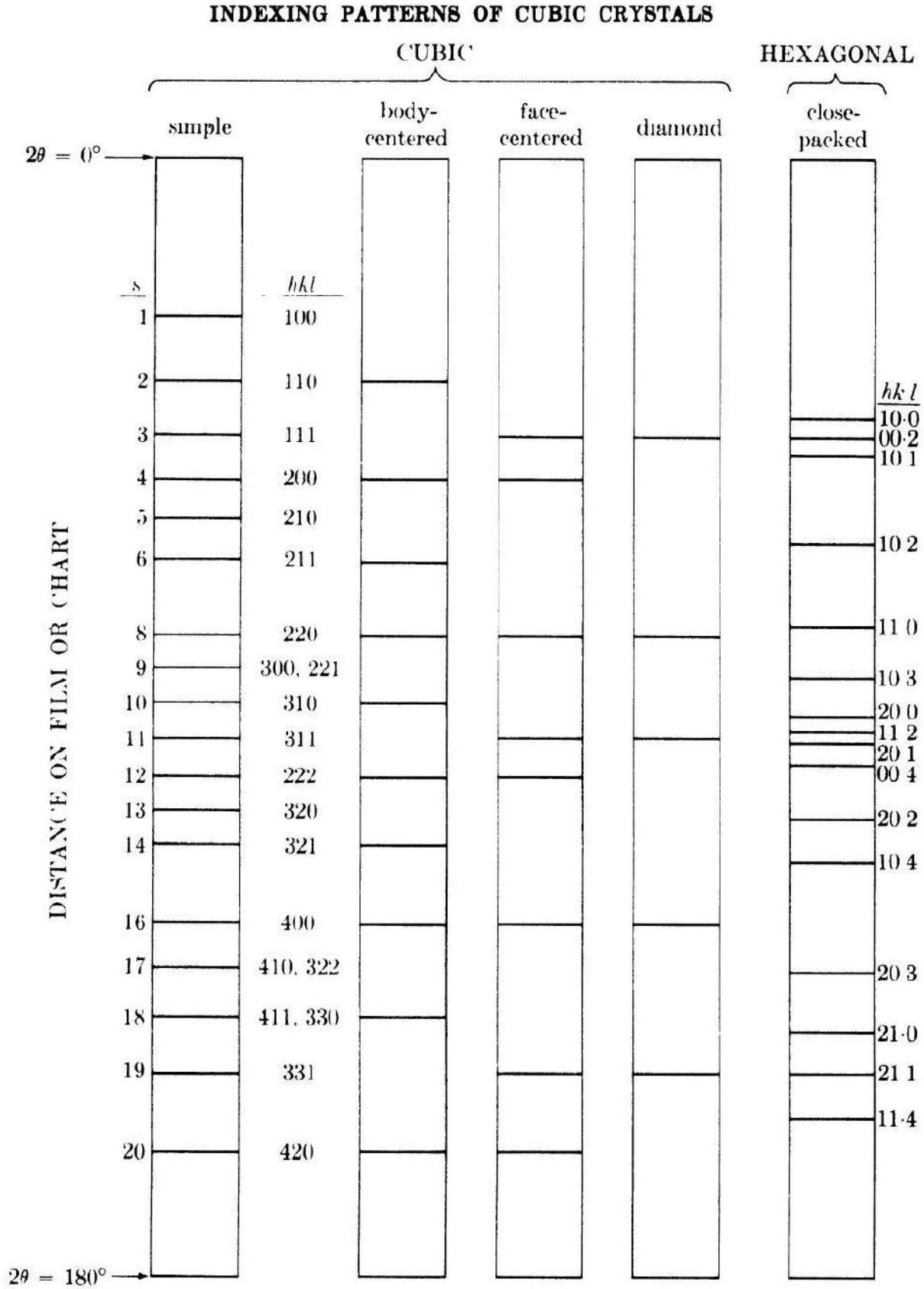

FIG. 10–2. Calculated diffraction patterns for various lattices. $s = h^2 + k^2 + l^2$

XRD Pattern of Al_2O_3

Comparing the obtained XRD pattern with the known standards in the JCPDS file for Al_2O_3, we can identify the crystal structure and phase identification is done especially comparing the first three highest intensity peaks. Following plots shows Al_2O_3 XRD pattern and JCPDS file for Al_2O_3 is also given.

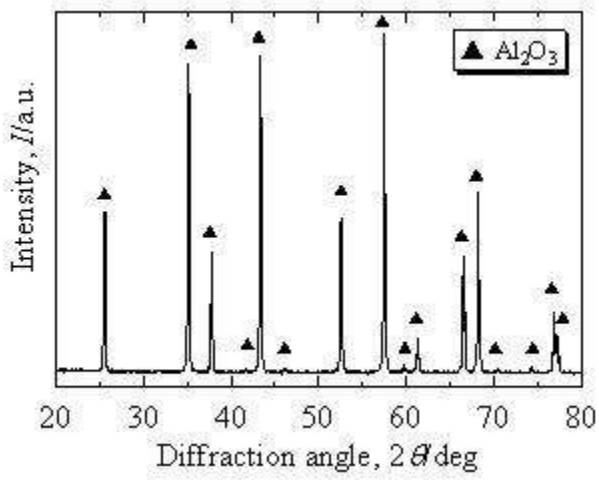

Name and formula

Reference code:	00-010-0173
Mineral name:	Corundum, syn
Common name:	alumina
PDF index name:	Aluminum Oxide
Empirical formula:	Al_2O_3
Chemical formula:	Al_2O_3

Crystallographic parameters

Crystal system:	Rhombohedral
Space group:	R-3c
Space group number:	167
a (Å):	4.7580
b (Å):	4.7580
c (Å):	12.9910
Alpha (°):	90.0000
Beta (°):	90.0000
Gamma (°):	120.0000
Calculated density (g/cm^3):	3.99
Measured density (g/cm^3):	4.05
Volume of cell (10^6 pm^3):	254.70
Z:	6.00
RIR:	1.00

Subfiles and Quality

Subfiles:	Inorganic Mineral Alloy, metal or intermetalic Cement and Hydration Product Corrosion Common Phase Educational pattern Forensic NBS pattern Superconducting Material
Quality:	Indexed (I)

Comments

Color:	Blue, colorless, yellow purple to violet, green, pink to deep pigeon-blood red
Sample preparation:	Sample annealed at 1400 C for four hours in an Al_2O_3 crucible.
Analysis:	Spectroscopic analysis showed <0.1% K, Na, Si; <0.01% Ca, Cu, Fe, Mg, Pb; <0.001% B, Cr, Li, Mn, Ni.
Optical data:	A=1.7604, B=1.7686, Sign=-
Additional pattern:	See ICSD 60419 (PDF 77-2135). To replace 43-1484.
Melting point:	2050°
Temperature:	Pattern taken at 26 C.

Peak list

No.	h	k	l	d [A]	2Theta[deg]	I [%]
1	0	1	2	3.47900	25.584	75.0
2	1	0	4	2.55200	35.137	90.0
3	1	1	0	2.37900	37.785	40.0
4	0	0	6	2.16500	41.685	1.0
5	1	1	3	2.08500	43.363	100.0
6	2	0	2	1.96400	46.184	2.0
7	0	2	4	1.74000	52.553	45.0
8	1	1	6	1.60100	57.519	80.0
9	2	1	1	1.54600	59.769	4.0
10	1	2	2	1.51400	61.166	6.0
11	0	1	8	1.51000	61.345	8.0
12	2	1	4	1.40400	66.548	30.0
13	3	0	0	1.37400	68.198	50.0
14	1	2	5	1.33700	70.359	2.0
15	2	0	8	1.27600	74.268	4.0
16	1	0	10	1.23900	76.882	16.0
17	1	1	9	1.23430	77.229	8.0
18	2	2	0	1.18980	80.695	8.0
19	3	0	6	1.16000	83.219	1.0
20	2	2	3	1.14700	84.378	6.0
21	1	3	1	1.13820	85.184	2.0
22	3	1	2	1.12550	86.378	6.0
23	1	2	8	1.12460	86.464	4.0
24	0	2	10	1.09880	89.021	8.0
25	0	0	12	1.08310	90.665	4.0
26	1	3	4	1.07810	91.204	8.0
27	2	2	6	1.04260	95.263	14.0
28	0	4	2	1.01750	98.410	2.0
29	2	1	10	0.99760	101.095	12.0
30	1	1	12	0.98570	102.792	1.0
31	4	0	4	0.98190	103.349	4.0
32	3	2	1	0.94310	109.526	1.0
33	1	2	11	0.94130	109.837	1.0
34	3	1	8	0.93450	111.033	4.0
35	2	2	9	0.91780	114.130	4.0
36	3	2	4	0.90760	116.146	14.0
37	0	1	14	0.90520	116.635	4.0
38	4	1	0	0.89910	117.906	8.0
39	2	3	5	0.88840	120.239	1.0
40	4	1	3	0.88040	122.077	4.0
41	0	4	8	0.86980	124.652	2.0
42	1	3	10	0.85800	127.737	12.0
43	3	0	12	0.85020	129.923	4.0
44	2	0	14	0.84600	131.155	4.0
45	1	4	6	0.83030	136.170	22.0
46	1	1	15	0.81370	142.405	4.0
47	4	0	10	0.80720	145.218	11.0
48	0	5	4	0.79880	149.298	7.0
49	1	0	16	0.79700	150.255	14.0
50	3	3	0	0.79310	152.457	13.0

Stick Pattern

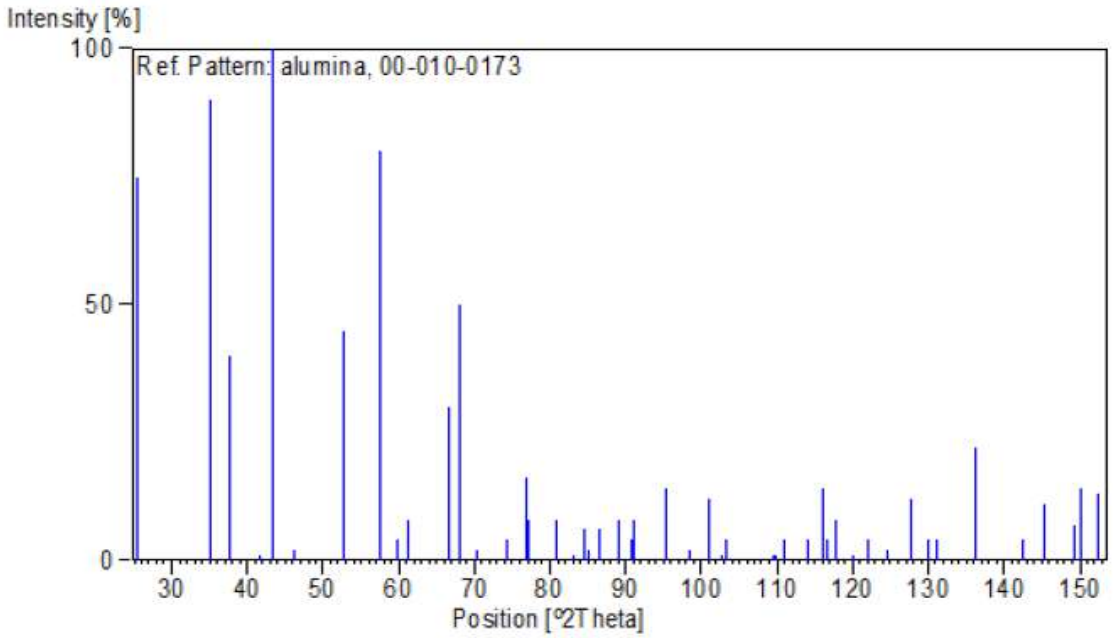

X-Ray Diffraction Analysis:

Bruker D8 ADVANCE diffractometer

Bruker-The New D8 ADVANCE All Purpose X-Ray Diffraction System

1. Lattice Parameter "a"

The lattice parameter "a" can be calculated from combination of Bragg law ($2d\sin\theta = n\lambda$) and d-spacing expression for cubic system using the formula

$$a = \sqrt{\frac{\lambda^2}{4\sin^2\theta}(h^2 + k^2 + l^2)}$$

Where λ is the wavelength of Cu kα radiation with 1.5405Å and θ is the diffraction Lattice constant.

2. Volume of the Cells

The volume of the unit cell can be calculated from the lattice parameters:

Crystal system	Unit Cell Volume
Cubic	$V = a^3$
Tetragonal	$V = a^2c$
Hexagonal	$V = a^2c\sin(60°)$
Trigonal	$V = a^2c\sin(60°)$
Orthorhombic	$V = abc$
Monoclinic	$V = abc\sin(\beta)$
Triclinic	$V = abc\,(1- \cos^2\alpha - \cos^2\beta - \cos^2\gamma) + 2(\cos(\alpha)\cos(\beta)\cos(\gamma))^{1/2}$

3. X-Ray Density

The x-ray density of material can be found by;

X-Ray Density = Weight of atoms in unit cell / Volume of Unit Cell

$$D_x = \frac{\sum A}{6.023\text{x}10^{23}\text{x}V^{1}\text{x}10^{-24}}$$

$$D_x = \frac{1.6603\ \sum A}{V}$$

where Dx = X-Ray Density = g/cm^3 and V = unit cell volume (A^o). Bulk density of the material is always less than the X-Ray density, because in bulk pores and holes are present.

4. Crystallite Size (Grain Size) (Size of Particle)

Crystallite size is different than particle size. A particle may be made up of several different crystallites. Crystallite size often matches grain size. The crystallite size is calculated by using Scherrer formula

$$\text{Crystallite Size (t)} = \frac{K\lambda}{B\cos\theta}$$

Where B is called full width half maximum (FWHM). Although the shape of crystallites is usually irregular, we often approximate them as spheres cube tetrahedral, octahedral, parallel piper or cylinders.

5. Bulk Density

Archimedean principle is applied for determining the bulk density of each sample. Each sample was immersed in toluene (liquid) and was exposed to the force buoyancy. The bulk density of the all sample under investigation was determined by the using the relation

$$\text{Bulk density} = \frac{\text{weight of the sample in air X density of toluene (liquid)}}{\text{Loss of weight of the sample in toluene (liquid)}}$$

$$\rho_B = \frac{W_s}{W_s - W_l} \times \rho_l$$

Where Ws is the weight of the sample in air , W_l is the weight of sample in toluene (liquid) and ρ_l is the density of toluene (liquid) .

6. Porosity

Porosity or void fraction is a measure of the void (i.e., "empty") spaces in a material, and is a fraction of the volume of voids over the total volume, between 0 and 1, or as a percentage between 0 and 100%. Porosity of a porous medium describes the fraction of void space in the material, where the void may contain, for example, air, water, some impurity or nothing. It is defined by the ratio:

$$\emptyset = \frac{V_v}{V_T} \times 100$$

where V_V is the volume of void-space and V_T is the total or bulk volume of material, including the solid and void components. Both the mathematical symbols ϕ and n are used to denote porosity. Porosity can be calculated with the help of bulk density ρ_B and x-ray density D_x as

$$\emptyset = \frac{D_x - \rho_B}{D_x} \times 100$$

7. Strain and Dislocation Density

Strain $\varepsilon = B \cos\theta /4$ and dislocation density $\delta = 1/t^2$ (lines $/m^2$) can be also calculated by using Williamson and Smallman's formula.

8. Volume Fraction of Phases Present in Samples

X-ray diffraction also allows a quantifiable measure of the volume fraction of phases present in a material.

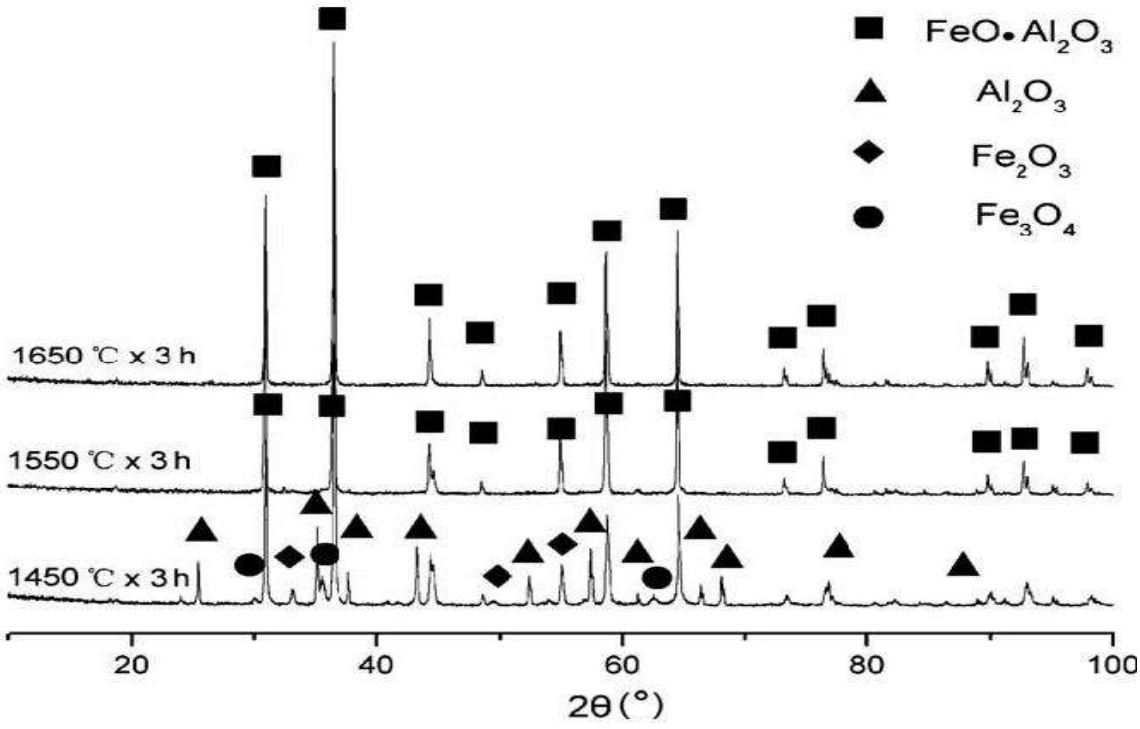
FeO•Al2O3
Al2O3
Fe2O3
Fe3O4
1650 ℃ x 3 h
1550 ℃ x 3 h
1450 ℃ x 3 h
20
40
60
80
100
2θ (°)

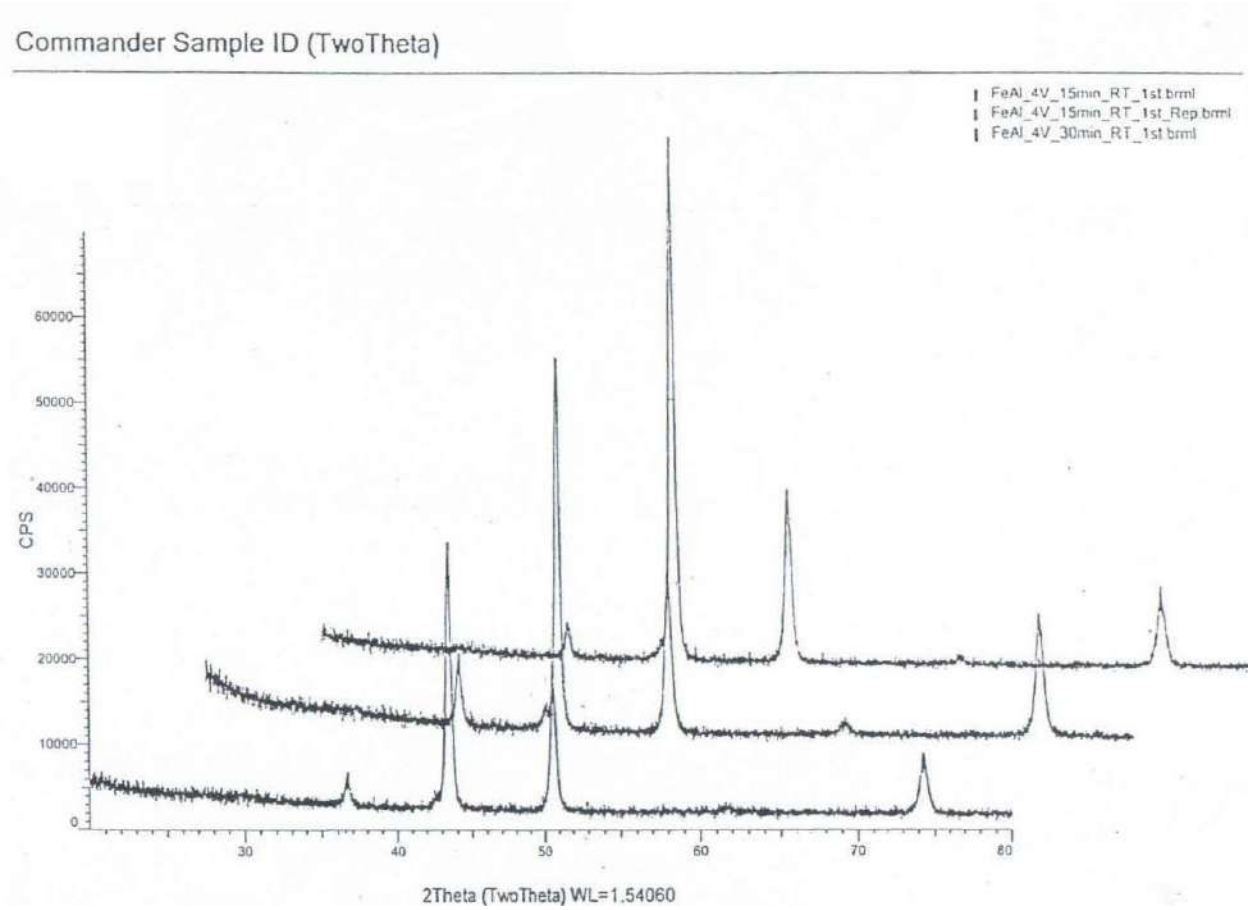

Sample No/Peaks with hkl	C (210)	Cu (111)	Fe (110) Al (200)	Cu (200)	Unknown	Cu (220)
1	36.7	42.5	43.7	50.5	61.5	74.3
2	36.8	42.5	43.5	50.5	61.5	74.4
3	36.6	42.6	43.3	50.5	61.5	74.3

Sample No.	**Fe-Al Peak 20 (degrees)**	**Interplanner spacing d (A^{o})**
1	43.7	2.0631
2	43.5	2.0722
3	43.3	2.0871

For Fe-Al

Sr No.	2θ (º)	d (A^o)	θ (º)	For Fe		For Al	
				hkl	a (A^o)	hkl	a (A^o)
1	43.7	2.0631	21.85	110	2.9268	200	4.1391
2	43.5	2.0722	21.75	110	2.9396	200	4.1572
3	43.3	2.0871	21.65	110	2.9525	200	4.1755

Sr No.	2θ (º)	FWHM 'B'		Crystallite Size $t=\frac{0.94\lambda}{B\ cos\theta}$ nm	Dislocation Density $\delta = 1/t^2$ lines/ m^2 10^{15}	Strain $\varepsilon = \frac{B\ cos\theta}{4}$ 10^{-3}
		(º)	(rad) 10^{-3}			
1	43.7	0.5	8.7266	17.894	3.123	8.099
2	43.5	0.4	6.9813	22.351	2.002	6.484
3	43.3	0.3	5.2359	29.782	1.127	4.867

Scanning Electron Microscopy (SEM)

Scanning electron microscope uses the electrons to scan the objects in a raster scan pattern. SEM is used to observe the surface texture and for measuring the thickness of grown films. SEM can give characteristic information about the topography, morphology, composition and crystallographic structure. Magnification of SEM can be achieved with the best of ~2 nm and it can be controlled over a range of upto 6 orders of magnitude from 10 to 500,000 times.

Working Principle: In scanning electron microscope (SEM) high energetic and focused electron beam is used to produce a variety of signals and images of the specimen surface. This variety of signals including secondary electrons, backscattered electrons, diffracted backscattered electrons, X- rays, visible light and heat are developed by electron-sample interactions. These signals especially secondary electrons and backscattered electrons are used to reveal different information about the sample.

Construction and working of SEM:

The major components of the SEM are

- Electron source
- Electromagnetic lenses
- Vacuum system: Chamber and gauge
- Sample stage
- Detector
- Display screen

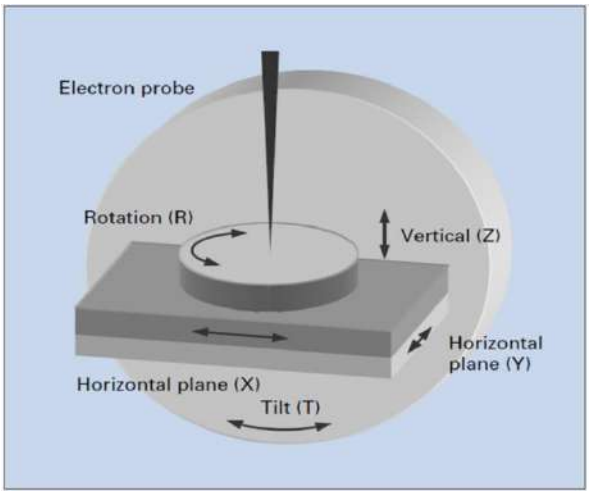

Figure: Sample stage with electron beam

Figure: The photograph of SEM with EDX (SEM Hitachi S-3400N)

A field emission gun generates electrons that are focused and accelerated towards the sample by several electromagnetic lenses. Accelerated electrons interact with the surface and cause the variety of electronic excitations. These electronic excitations include the secondary electrons, scattered electrons, diffracted electrons, photons, visible light and heat. A negative potential is provided to focus and control the emission of electrons as a narrow beam. The electron beam is guided to the electron column by a series of electromagnetic lenses. The condenser and objective lenses are used to adjust the focusing, spot size and the resolution. The electrons interact with the sample within a very short time. Back scattered and secondary electrons are emitted from the sample primarily. Secondary electrons and backscattered electrons are used for imaging the samples once these electrons escape from the sample surface; they are typically detected by detector. The SEM image formed as a result of the intensity of the secondary electron emission from the sample at each x, y data point during the rastering of the electron beam across the surface.

Sample Preparation for SEM: For conventional imaging in SEM, specimens must be electrically conductive at least at the surface. The operating environment of SEM dictates that specialist preparation techniques are used. Typically, a biological specimen is chemically fixed (fixation: incubation in a buffered solution), dehydrated through an acetone or ethanol series and then dried at the critical point -a method used to minimize specimen distortion due to drying tensions. For dry samples, this process is not necessary. Electrically insulating sample may need to be coated with gold, graphite or palladium to stop charge building up on the surface. Typically coating is applied using a **sputter coater**. SEM can also be used to investigate smooth surfaces of industrial samples.

SEM and EDS analysis of hercynite ($FeO{\cdot}Al_2O_3$ or $FeAl_2O_4$)

The microstructure morphology of the specimen fired at 1450 ◦C is shown in Fig. 2a. The specimen contained white particles and did not have a dense structure. According to the EDS analysis, the white spherical particles were Fe_3O_4 or Fe_2O_3 (Fig. 2b), whereas the gray parts were hercynite (Fig. 2c). No octahedral or cubic hercynite was observed. Figs. 3 and 4 show the morphology of sectioned specimens sintered at 1550 ◦C and 1650 ◦C. These specimens had dense structures and well-grown hercynite crystals. The crystal structure of as-prepared hercynite is typically octahedral or cubic after being fired at 1550 ◦C or above, which is consistent with the crystallisation law of hercynite. The hercynite crystals connected with each other, indicating that the hercynite synthesised using this method was of high purity.

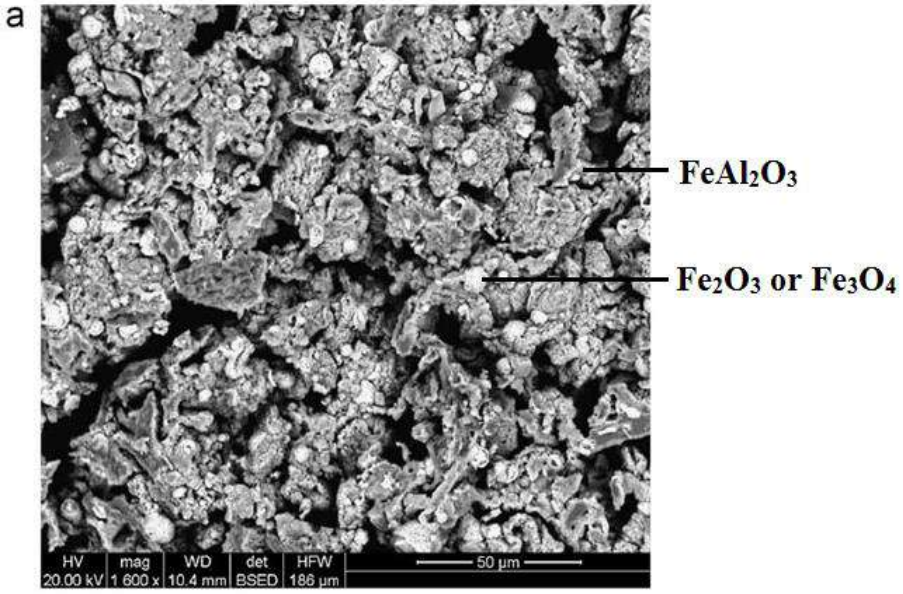

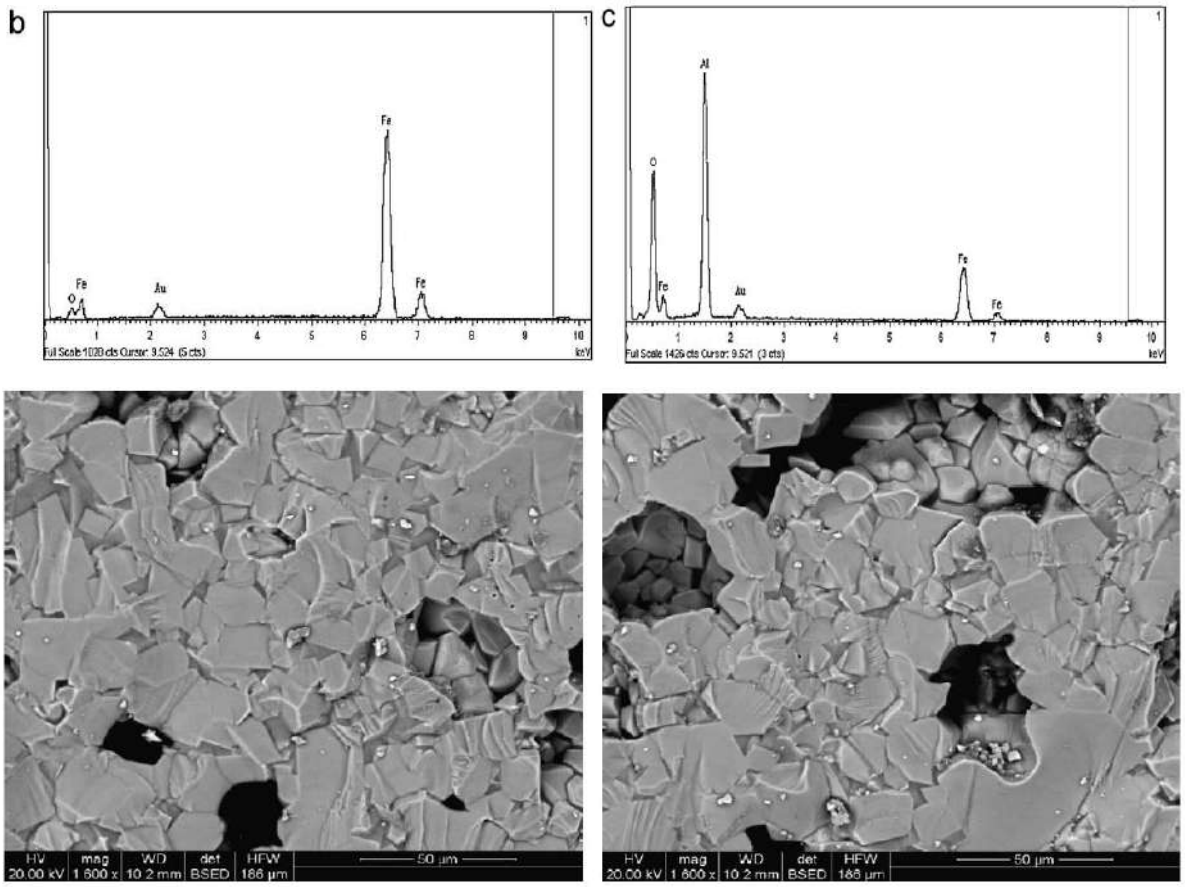

Fig. 3. SEM photograph of the specimen fired at 1550 °C.

Fig. 4. SEM photograph of the specimen fired at 1650 °C.

The microstructures of highly pure hercynite ($FeO \cdot Al_2O_3$ or $FeAl_2O_4$) examined by SEM (SEM; Quanta200, FEI, Holland) equipped with energy dispersive spectroscopy (EDS; INCA250 Oxford Instruments, UK).

Energy-dispersive X-ray spectroscopy (EDS or EDX)

Energy-dispersive X-ray spectroscopy (EDS, EDX, or XEDS), sometimes called energy dispersive X-ray analysis (EDXA) or energy dispersive X-ray microanalysis (EDXMA), is an analytical technique used for the elemental analysis or chemical characterization of a sample.

Working Principle: It relies on an interaction of X-rays with the sample. Its characterization capabilities are due in large part to the fundamental principle that each element has a unique set of peaks on its X-ray emission spectrum. These peaks are called characteristic X-rays of the atoms in the sample. In EDX, these characteristic x-rays are used to identify the elements.

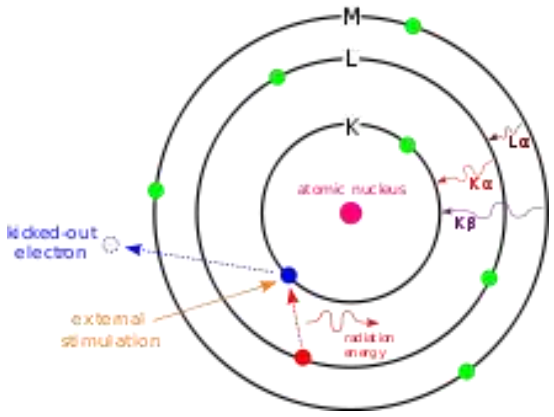

Construction and Working:

Four primary components of the EDS setup are

1. the excitation source (electron beam or x-ray beam)
2. the X-ray detector
3. the pulse processor
4. the analyzer.

To stimulate the emission of characteristic X-rays from the sample, a high-energy beam of electrons or a beam of X-rays, is focused into the sample being studied. At rest, an atom within the sample contains ground state (or unexcited) electrons in discrete energy levels or electron shells bound to the nucleus. The incident beam may excite an electron in an inner shell, ejecting it from the shell while creating an electron hole where the electron was. An electron from an outer, higher-energy shell then fills the hole, and the difference in energy between the higher-energy shell and the lower energy shell may be released in the form of an X-ray. These X-rays are separated by a Si-Li detector and amplified and corrected for absorption. The number and energy of these X-rays can be measured by an energy-dispersive spectrometer. A detector is used to convert X-ray energy into voltage signals; this information is sent to a pulse processor, which measures the signals and passes them onto an analyzer for data display and analysis. As the energy of the X-ray is characteristic of the difference in energy between the two shells, and of the atomic structure of the element from which they were emitted, this allows the elemental composition of the specimen to be measured. EDS works best for elements Na and heavier. It is used for quantitative analysis. It can be used with SEM. It gives information about chemical composition of different parts on the SEM micrograph of the sample. For example, the spectrum below is of a high temperature nickel based alloy composed of nickel, chromium, iron, manganese, titanium, molybdenum, silicon, and aluminum. It also gives weight % of the element present in the alloy.

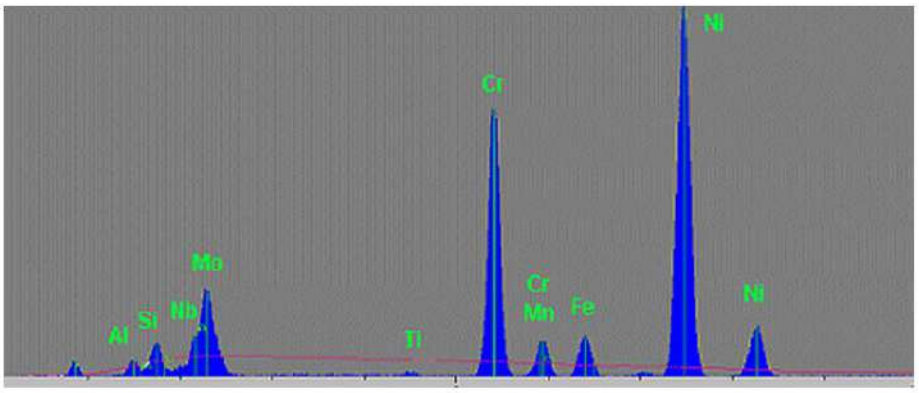

The SEM-EDS analysis of a specimen is shown in Fig. a, b and c. The specimen contained white particles and did not have a dense structure. According to the EDS analysis, the white spherical particles were Fe_3O_4 or Fe_2O_3 (Fig. b), whereas the gray parts were hercynite (Fig. c).

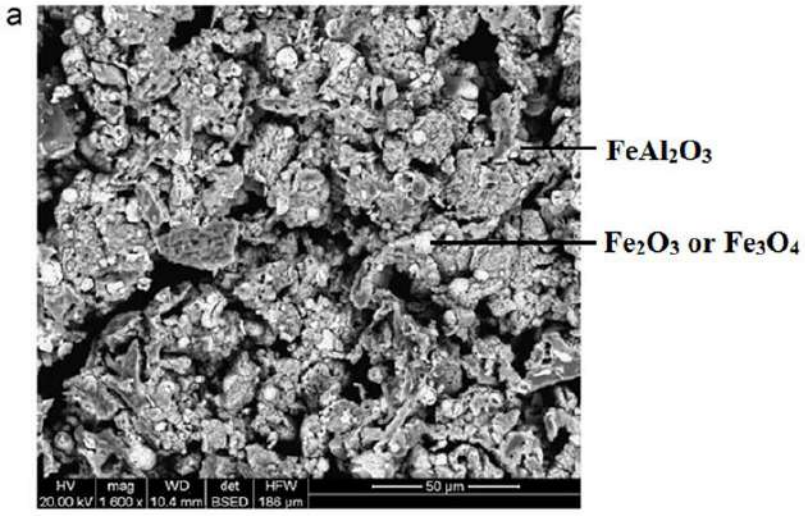

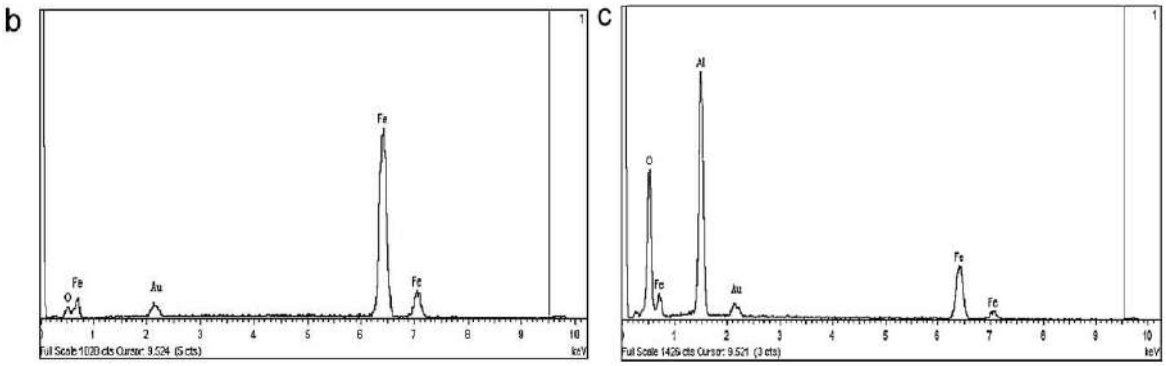

Transmission Electron Microscopy

Transmission electron microscopy (TEM) is a microscopy technique in which a beam of electrons is transmitted through an ultra-thin specimen, interacting with the specimen as it passes through. An image is formed from the interaction of the electrons transmitted through the specimen. High resolution microscopy uses a very high potential field (106 V), which results in very short wavelengths. TEM/HREM images bulk structure and can detect crystal defects, phase boundaries, shear planes, etc. A resolution of ~0.5 nm can be achieved.

Working Principle: TEM requires a thin (~200 nm) sample that is subjected to a high energy, high intensity beam of electrons. Electrons that pass through the sample are detected forming a two dimensional projection of the sample. Electrons may be elastically or inelastically scattered and the instrument may be operated in the direct (bright field) or diffracted beam (dark field).

Construction and Working:

There are four parts for a transmission electron microscope:

- Vacuum system
- Electron source
- Electromagnetic lens system
- Sample holder
- Imaging system

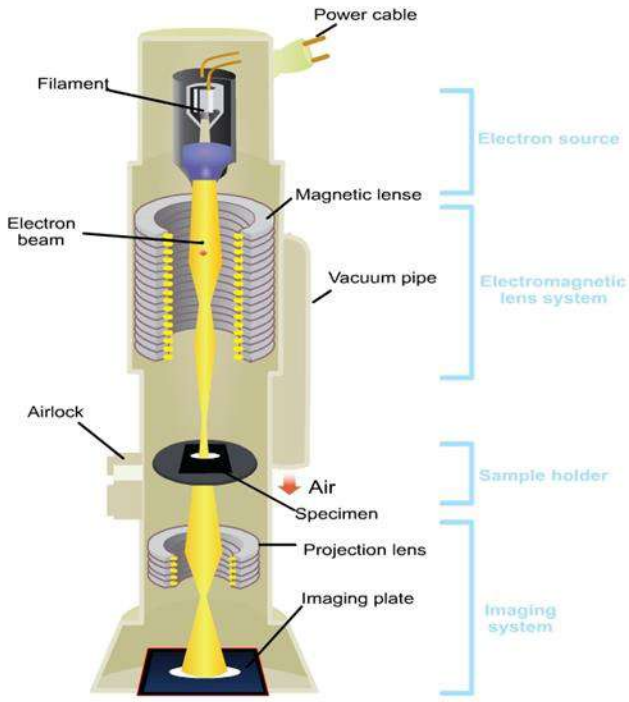

The electron source is an electron gun which consists of a tungsten filament. This filament emits electrons when it is heated through the phenomenon of thermionic or field emission. The beam of electrons is the focused on the specimen by the condenser which consists of electromagnetic lenses. The sample holder consists of a mechanical arm which holds the specimen. The imaging system also consists of electromagnetic lens system and a screen which has a phosphorescent plate. The plate glows when hit by the electrons after passing through the specimen. The whole systems of electron source, electromagnetic lenses and sample holder are enclosed in vacuum. Air must be evacuated from the column to create a vacuum so that the collision of electrons with air molecules and hence the scattering of electrons are avoided. The electrons beam is focused to the sample and it passes through the specimen and scattered by the internal structures. TEM involves a high voltage beam of electrons emitted by a cathode and formed by magnetic lenses. The beam of electron that has been partially transmitted through the very thin specimen carries information about the structure of the specimen and the beam of electrons is recorded with the help of a detector. The spatial variation in this information ("image") is then magnified by a series of magnetic lenses until it is recorded by CCD (charge-coupled device) camera. The image detected by the CCD may be displayed in real time on a monitor or computer.

Sample Preparation

Sample preparation in TEM can be a complex procedure. TEM specimens are required to be at most hundreds of nanometers thick. High quality samples will have a thickness that is comparable to the mean free path of the electrons that travel through the samples, which may be only a few tens of nanometers. Preparation of TEM specimens is specific to the material under analysis and the desired information to obtain from the specimen. As such, many generic techniques have been used for the preparation of the required thin sections.

- Materials that have dimensions small enough to be electron transparent, such as powders or nanotubes, can be quickly prepared by the deposition of a dilute sample containing the specimen onto support grids or films.
- In material science and metallurgy the specimens tend to be naturally resistant to vacuum, but still must be prepared as a thin foil, or etched so some portion of the specimen is thin enough for the beam to penetrate.
- In the biological sciences in order to withstand the instrument vacuum and facilitate handling, there are different steps involves for sample preparation Processing, embedding, polymerization and sectioning.

1. Processing: Processing includes: fixation, rinsing, post fixation, dehydration and infiltration.

a) **Fixation:** This is done to preserve the sample and to prevent further deterioration so that it appears as close as possible to the living state, although it is dead now. It stabilizes the cell structure. There is minimum alteration to cell morphology and volume.

b) Rinsing: The samples should be washed with a buffer to maintain the pH in the buffering range of 5.1-7.4.

b) **Post Fixation:** A secondary fixation is used to increase the stability and contrast of fine structure.

d) Dehydration: The water content in the tissue sample should be replaced with an organic solvent since the epoxy resin used in infiltration and embedding step is not miscible with water.

c) **e) Infiltration:** Epoxy resin is used to infiltrate the cells. It penetrates the cells and fills the space to give hard plastic material which will tolerate the pressure of cutting.

2. Embedding: After processing the next step is embedding. This is done using flat molds.

3. Polymerization

Next is polymerization step in which the resin is allowed to set overnight at a temperature of 60 degree in an oven.

4. Sectioning

The specimen must be cut into very thin sections for electron microscopy so that the electrons are semi-transparent to electrons. These sections are cut on an ultramicrotome which is a device

with a glass or diamond knife. For best resolution the sections must be 30 to 60 nm.

The resin block can be made ready for the sectioning by trimming it at the tip with a razor blade or black trimmer so that the smallest cutting face is available. Fix the block to a microtome and cut the sections. Sections float onto a surface of liquid held in trough and remain together in a form of ribbon. Freshly distilled water is generally used to fill the trough. These sections are then collected onto a copper grid and viewed under the microscope.

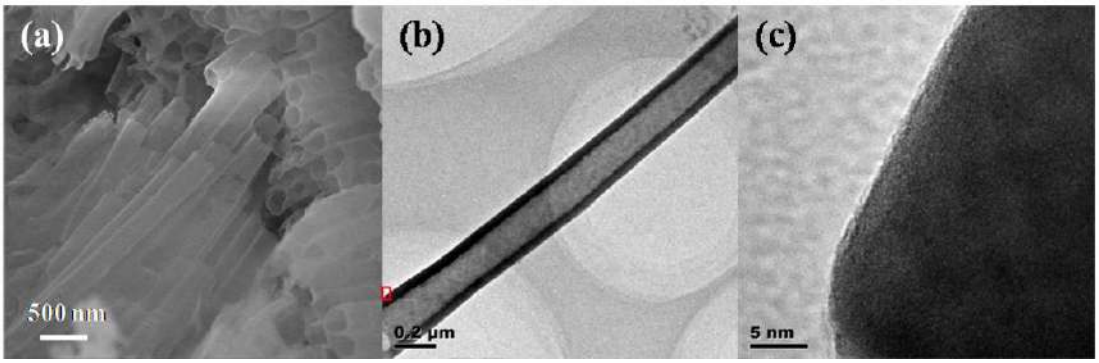

Figure: SEM, TEM, and HRTEM images of (a)-(c) La-Co nanotubes respectively

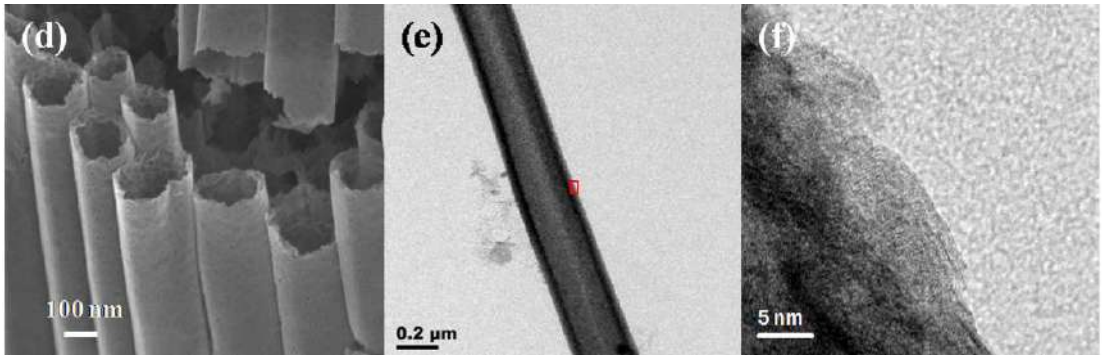

Figure: SEM, TEM, and HRTEM images of (d)-(f) La-Ni nanotubes respectively

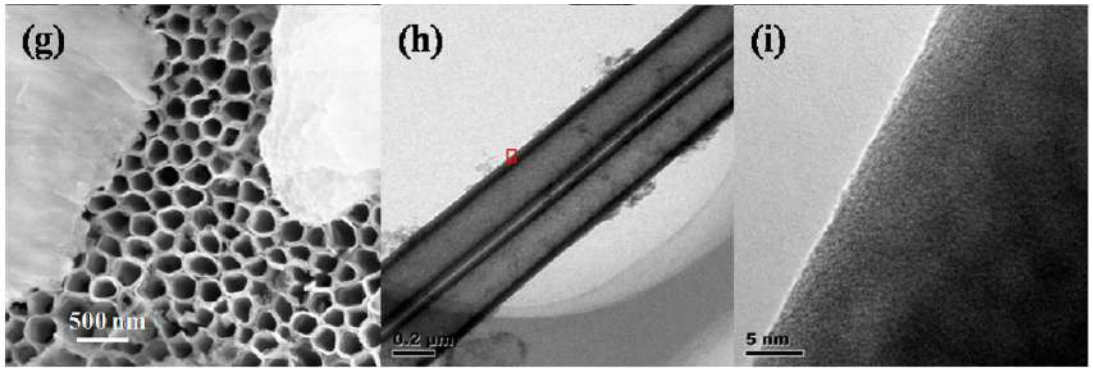

Figure: SEM, TEM, and HRTEM images of (g)-(i) La-Fe nanotubes respectively

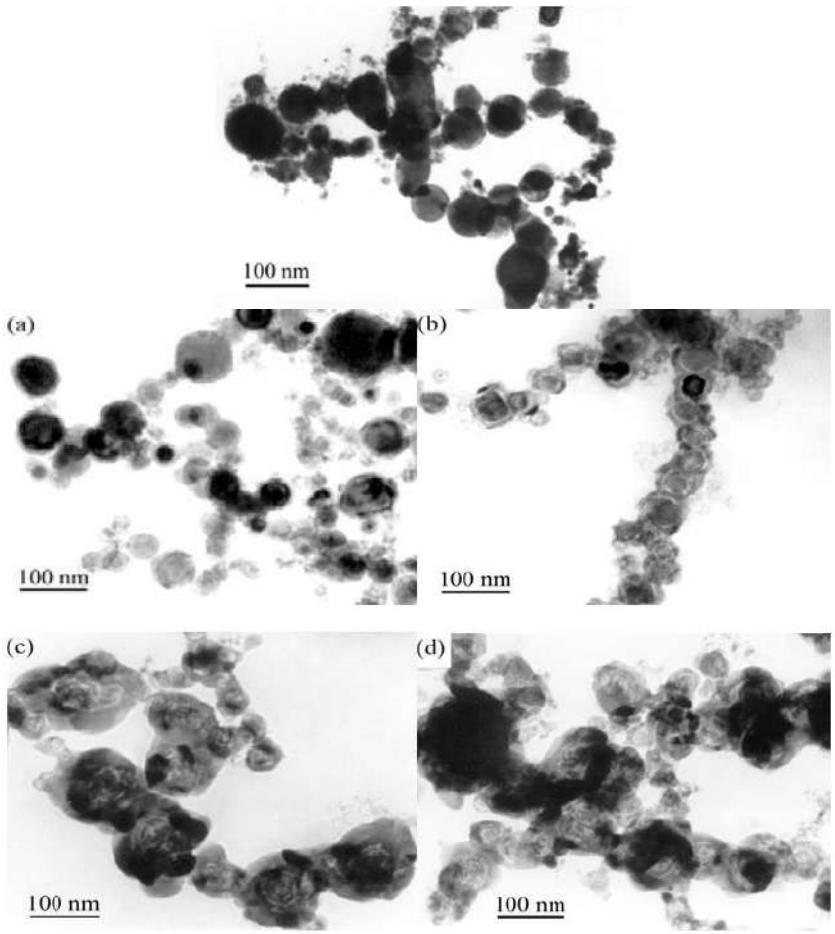

TEM bright field images of Fe_3Al nanoparticle samples first as-prepared by hydrogen plasma–metal reaction and heated at (a) 473 K, (b) 573 K, (c) 673 K and (d) 873 K.

TEM bright field images of Fe_3Al nanoparticles heated at different temperatures are given above. There is no neck formation between particles heated at 473 K (figure(a)). Thin layers about 5 nm in thickness occur around the nanoparticles, which is crystallized iron oxide (XRD). It seems that the shapes of the Fe_3Al nanoparticles are stable at that temperature. The nanoparticles with shell structure start to coalesce by neck growth at 573K (figure (b)). This grey shell grows thicker due to a small amount of Fe_3Al oxidation, and a new white layer, assumed to be alumina, appears between the core and the grey shell. The morphology of the nanoparticles grows to a multiple-layer style at 673 K (figure (c)) and the boundary between nanoparticles disappears owing to the high energy released during the oxidation. The multiple-layer morphology becomes less obvious at 873 K (figure (d)). It is found that mean particle size grows larger than 100 nm above 673 K owing to the coalescence and oxidation expansion of the spherical nanoparticles.

Difference between SEM and TEM

Both SEM and TEM detect the electrons that emitted from the surface of the sample.

The accelerated voltage is ranging from 10kV to 40kV for the SEM. The thickness of the specimen in this case is not important. In addition, the samples to be tested have to be electrically conductive; otherwise they would be overcharged with electrons. However, they can be coated with a conductive layer of metal or carbon.

In TEM, the transmitted electrons are detected, and in this case the specimen thickness is important and typically should not exceed 250 nm (0.25μm). The accelerated voltage in this case is less than 100kV.

Atomic Force Microscopes (AFM)

All of these microscopes provide 3-D topographic information about a sample by measuring a local property with a tip placed very close to the sample. The tip is scanned laterally across the surface, and the vertical movements of the tip are recorded and the tip-sample separation (on the order of the instrument's resolution) makes it possible to take measurements over a small area resulting in a raster image. The lateral resolution of the image can be as small as the tip radius (typically 5-15 nm), and the vertical resolution can be on the order of angstroms.

Principle:

AFM is based on the existence of a separation-dependency force between any two bodies. It is the force between the tip and the sample surface that is present at close separations. Typically, few nanometer pyramidal silicon nitride tips are used. The force is detected by placing the top on a flexible cantilever that deflects proportionally to the exerted force. The deflection is then measured by some convenient procedure, such as laser light deflection or some other device. The deflection reflects the surface morphology and properties to construct a 3-D image of the sample surface.

In **contact mode**, AFM operates by measuring attractive or repulsive forces between a tip and the sample. In its repulsive "contact" mode, the instrument lightly touches a tip at the end of a leaf spring or "cantilever" to the sample. As a raster-scan drags the tip over the sample, some sort of detection apparatus measures the vertical deflection of the cantilever, which indicates the local sample height. Thus, in contact mode the AFM measures hard-sphere repulsion forces between the tip and sample.

In **noncontact mode**, the AFM derives topographic images from measurements of attractive forces; the tip does not touch the sample. AFMs can achieve a resolution of 10 pm, and unlike electron microscopes, it can image the samples both in air and under liquids. A unique advantage of AFM is that it enables imaging with minimal sample preparation, in air or liquid environment.

Construction:

In principle, AFM resembles the record player. Figure shows the schematic construction of AFM. However, AFM incorporates a number of refinements that enable it to achieve atomic-scale resolution:

- Sensitive detection
- Flexible cantilevers
- Sharp tips
- High-resolution tip-sample positioning
- Force feedback

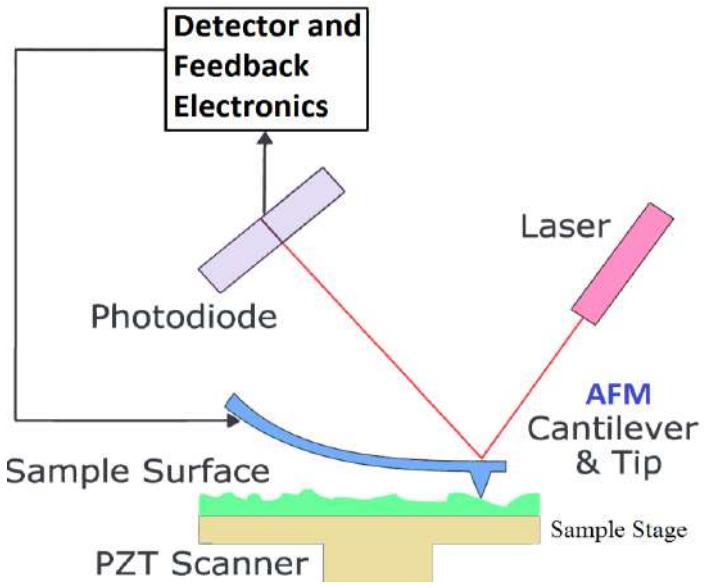

Figure: Scanning Probe Microscopy with AFM and STM Heads

Technical Advantages:

- Quantitative 3-D images with a resolution of 10 pm
- Topographical information at high lateral resolution
- Direct Image formation both in air and under liquids
- Little or no sample prep in many cases
- Little to no harm to sample
- Applicable to conductive and insulating materials
- Characterization of nanoparticles that are .5 nm in diameter and larger.
- Nanoparticle mixture distributions below 30 nm.
- Characterization of variable geometry nanoparticles.
- Characterization of nanoparticle physical properties such as magnetic fields.

Typical Applications:

- High-resolution surface profilometry (grain size and grain distribution)
- Surface roughness(Smoothness) measurements
- Microstructural studies of metallic, ceramic, semiconducting and polymeric materials
- Defect and failure analysis
- Pit analysis for optical disk storage media
- Magnetic domain and surface roughness analysis for computer hard-disks
- Semiconductor device structural analyses
- Surface cleaning and polishing studies
- Phase separation in polymers
- Critical Dimension Measurements
- Investigation of local mechanical properties (i.e. stiffness, adhesion, friction)
- High-resolution imaging of biological samples
- Studies of nano-scale forces

Instrumentation:

- Sample Size: diameter of samples up to 100-210mm and thickness ≤15mm
- Resolution along x and y: 2-5nm,
- Resolution along z: 0.05-1nm
- X-Y Position Noise: ≤ 0.15nm RMS typical imaging bandwidth (up to 625Hz)
- Z Sensor Noise Level: 35pm RMS typical imaging bandwidth (up to 625Hz)
- X-Y Imaging Area: 90µm x 90µm
- Z range: 5-10µm
- Modes: different modes in different models

Sample Preparation and Inspection

Reference materials used for the sample preparation (deposition) consist of negatively surface charge or zeta potential. Nanoparticle samples need to be dispersed on flat surfaces for AFM

measurements. The roughness of the surface should be much less than the nominal size of the nanoparticles in order to provide a consistent baseline for height measurements. High-quality mica (mica is a cleaned layered mineral or atomically flat surfaces), atomically flat gold (111) (deposited on mica), or single crystal silicon can all be used as substrates to minimize the effect of surface roughness on nanoparticle measurements. Inspect each sample using an optical microscope before AFM imaging to find possible areas where one can expect a reasonably good dispersion of the particles. In most cases, the exterior of the dried droplet includes excess stabilizing agents, while the interior is free of these agents with suitable particle distributions.

AFM provides a three-dimensional surface profile where the lateral (x and y) dimensions are influenced by the shape of the probe and the height (vertical, z) measurements can provide the height of nanoparticles with a high degree of accuracy and precision. If particles are assumed to be spherical, the height measurement corresponds to the diameter or size of the particle.

AFM Imaging and Size Measurement Procedure

In order to obtain accurate measurements, the axial (z)-displacement of the piezoelectric stage needs to be calibrated using available traceable standards. After choosing a suitable grating (the step height of the grating should be similar to the characteristic height of the nanoparticles), measure the calibration grating in several locations using a sharp AFM tip and compare the average measured value to the certified step height. Nanoparticles are fixed to the substrate via weak forces (*e.g.*, electrostatic and van der Waals forces). As a result, intermittent contact mode is a suitable imaging mode in which the cantilever is driven to oscillate up and down near its resonance frequency by a small piezoelectric element mounted in the AFM tip holder. The amplitude of this oscillation is greater than 10 nm, typically 100 nm to 200 nm.

Probes consist of a cantilever integrated with a sharp tip on the end. The properties and dimensions of the cantilever and sharp tip play an important role in determining the sensitivity and resolution of the AFM. Stable cantilever oscillations are required to successfully image a surface in intermittent contact mode, and are only possible when the cantilever has stiffness 40 Nm^{-1} to overcome adhesive forces between the tip and sample. In most AFM instruments, the cantilever itself is tilted by 10° to

20° relative to the surface. This is to ensure that the tip makes contact with the sample before any other component.

AFM images have a lateral (x, y) resolution and a vertical (z) resolution. The radius of curvature of the end of the tip will determine the highest lateral resolution obtainable with a specific tip. However, another factor that needs to be considered during image analysis is the number of data points, or pixels, present in an image in the x and y scan-direction. Thus, it is important to consider the particle size when choosing the scan size.

After completing the general setup for the AFM, at first, use a large scan size to identify a region with a homogeneous nanoparticle distribution. Once a suitable region has been identified, start collecting the nanoparticle images, using the scan parameters above as a starting point. Adjust the oscillation amplitude feedback gains to ensure that the forward and backward line scans look identical. Store the images on the computer with incremental filenames for post-imaging analysis.

Once images are captured, they can be viewed, modified, and analyzed offline using the software supplied by the AFM manufacturer. Most AFM software packages offer an automated particle analysis function. The software can measure the height of particles based on the height of pixel data by using the threshold method and plot a histogram distribution. After selecting a group of particles, the distance between the maximum height of pixel data from individual particles and substrate can be automatically measured, and the height mean value and standard deviation of particles can be calculated.

Qualitative Analysis by AFM

Using the AFM, individual particles and groups of particles can be resolved. The AFM offers visualization in three dimensions. Resolution in the vertical, or Z, axis is limited by the vibration environment of the instrument: whereas resolution in the horizontal, or X-Y, axis is limited by the diameter of tip utilized for scanning. Typically, AFM instruments have vertical resolutions of less than 0.1 nm and X-Y resolutions of around 1 nm.

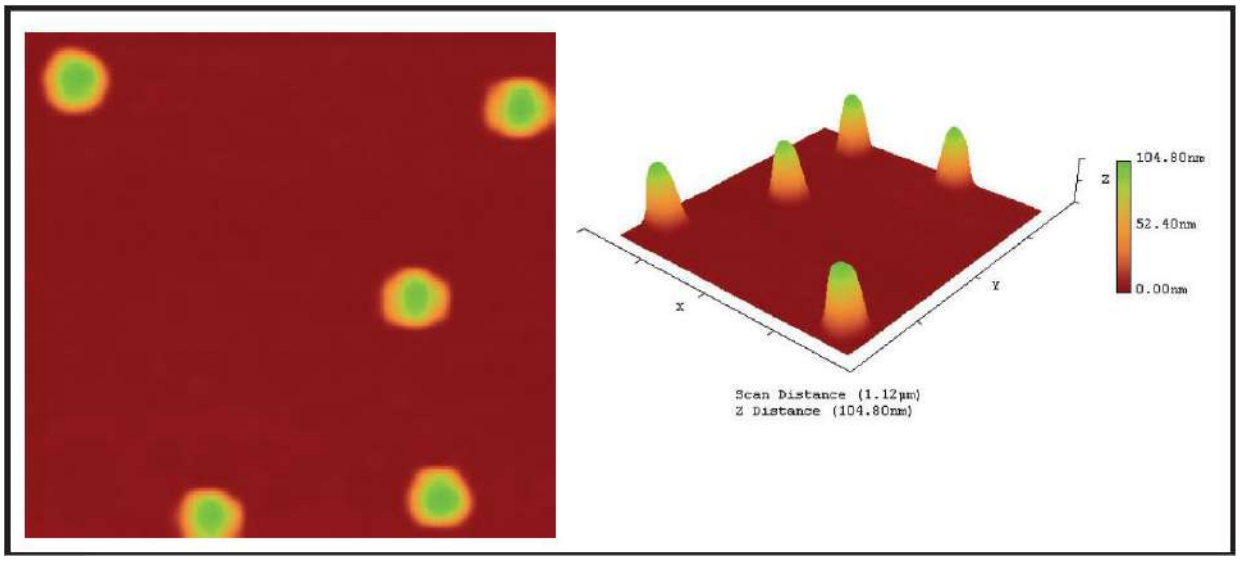

In Figure above, 73nm NIST traceable microspheres are shown in both perspective view and top view. 3D information is incorporated in both views. In the perspective view, the 3D nature of the image is obvious. In the top view, the intensity of the color reflects the height of the particle.
In material sensing mode, the AFM can distinguish between different materials, providing spatial distribution information on composite materials with otherwise uninformative topographies.

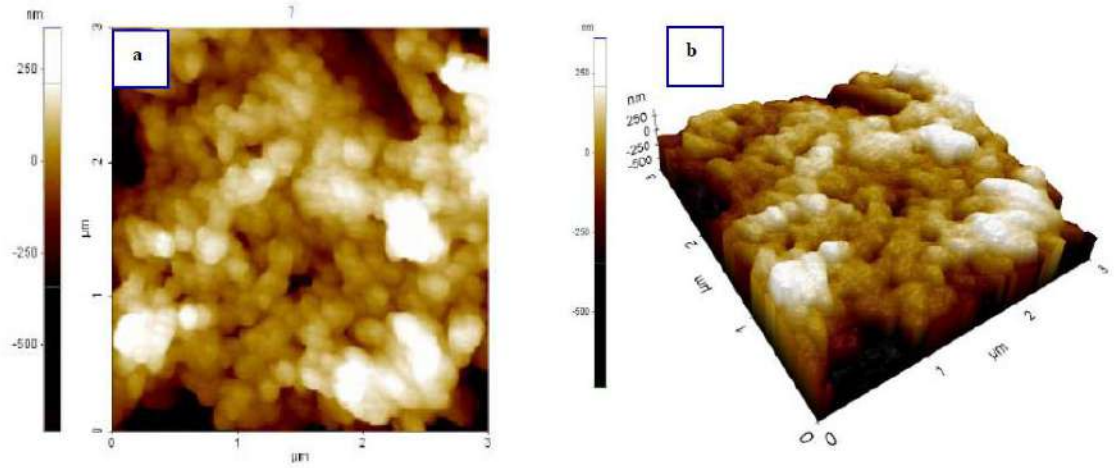

Figure 2. AFM images of TiO_2 thin films sintered at 700^{0}C for 1 hr in air. a) Planer view; b) 3D view.

Quantitative Analysis by AFM

Software-based image processing of AFM data can generate quantitative information from individual nanoparticles and between groups of nanoparticles. For individual particles, size information (length, width, and height) and other physical properties (such as morphology and surface texture) can be measured. Statistics on groups of particles can also be measured through image analysis and data

processing. Commonly desired ensemble statistics include particle counts, particle size distribution, surface area distribution and volume distribution. With knowledge of the material density, mass distribution can be easily calculated.

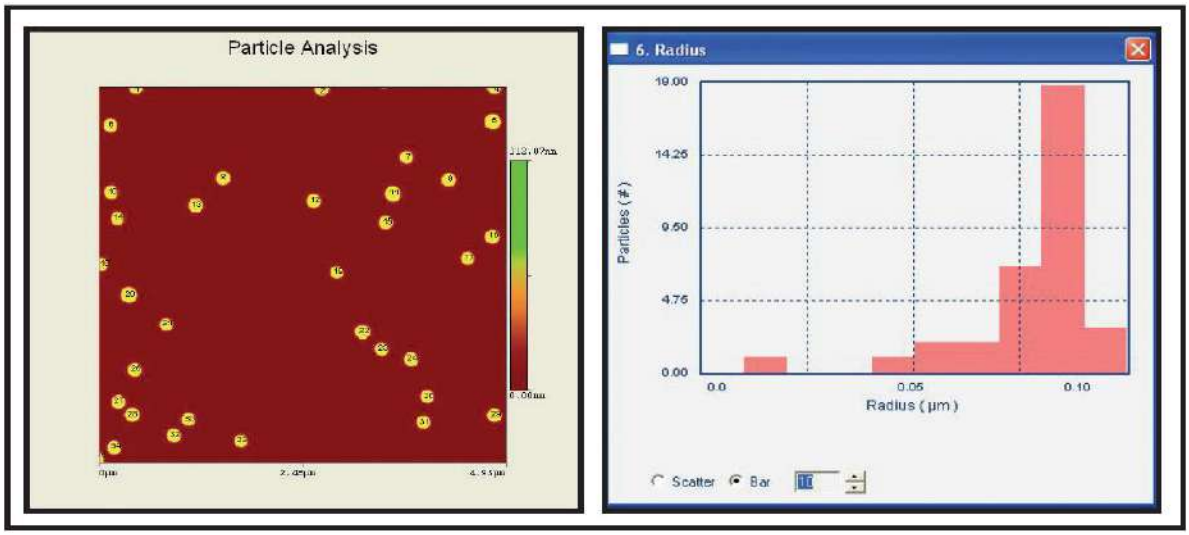

Image processing of an AFM image is shown in Figure above. In the figure, left: Latex particles outlined and counted, right: Particle size distribution of polymer nanoshperes. Whenever data from single-particle techniques is processed to provide statistical information, the concern over statistical significance exists. It is easy to attain greater statistical significance in AFM by combining data from multiple scans to obtain information on the larger population.

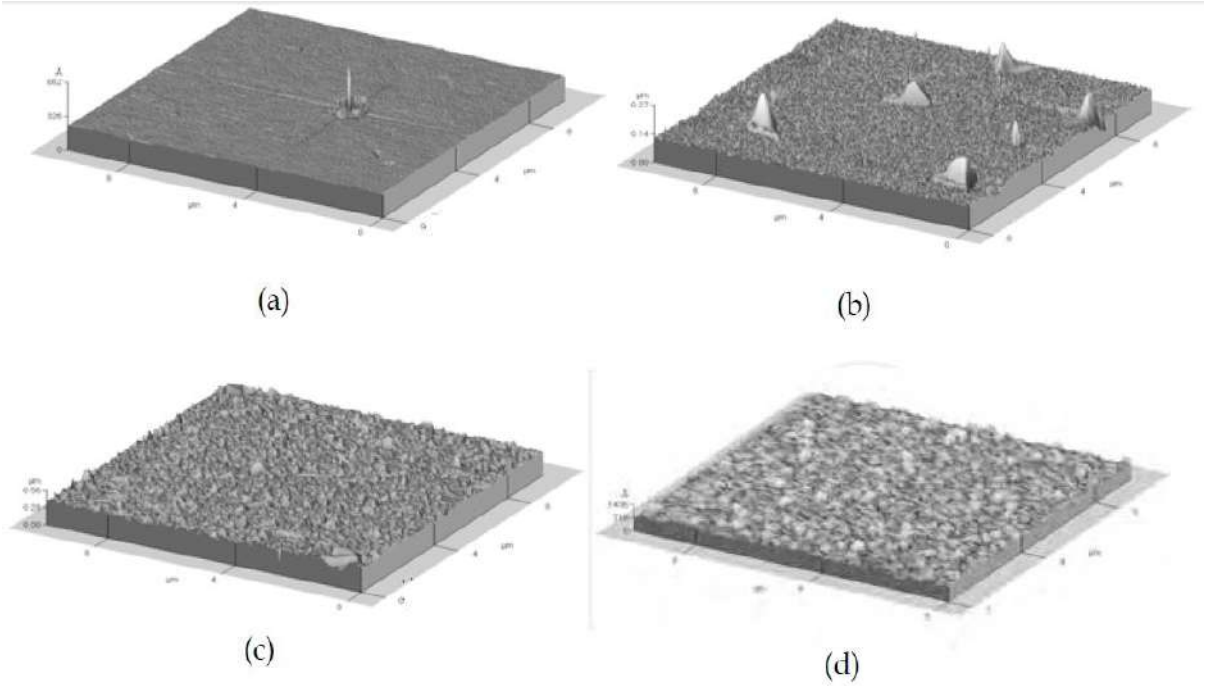

Figures above shows AFM images of the as-cast thin film and the thin films deposited at 200 W and annealed at different temperatures for 30 min, (a) as-cast, (b) 850 oC, (c) 1000 oC, (d) 1150 oC. The grains on the surface of the samples become greater gradually with the increase of annealing temperature, which indicates that surface morphology and crystallization of the grains depend on annealing temperature significantly – the higher the annealing temperature, the better the morphology and crystalline quality. Besides, the thin film surface becomes rougher with the increase in annealing temperature.

Magnetization Process in Ferro (ferri) Magnets

When we draw a graph between the magnetization, M, or magnetic flux density, B, and externally applied field, H, we get linear relationship for diamagnetic and paramagnetic materials while ferromagnetic (ferrimagnetic) materials show non-linear relation and form **hysteresis curve** as shown in figures below. The hysteresis curve is just a schematic representation.

For ferromagnets, initially the magnetic moments of all the constituent domains are randomly oriented with no net *B (or M)* field. The magnetic polarization of the magnetic material sample increases when an external magnetic field is applied to an un-magnetized magnetic material sample. Well oriented magnetic moments of the domains nucleate and then rotate along the easy direction of the crystal. When the increase in the magnetic moments of the domains approaches maximum, the direction of moments of the domains rotates away from the easy axis to align with the applied field. When all of the domains within the sample have fully aligned magnetic moments with the applied field, saturation is reached and no further increase occurs in the magnetic polarization. At this stage, the magnetization is called as **saturation magnetization** or **spontaneous magnetization, $\mathbf{M_s}$**. The resultant M (H) curve is called the initial magnetization curve. When the applied field is decreased to zero, the curve does not retrace its original path. The material will still have some magnetization due to the remaining flux density and this flux density is known as the **remanence ($\mathbf{M_r}$)** of the magnetic material. It indicates that the material remains magnetized even in the absence of the external field.

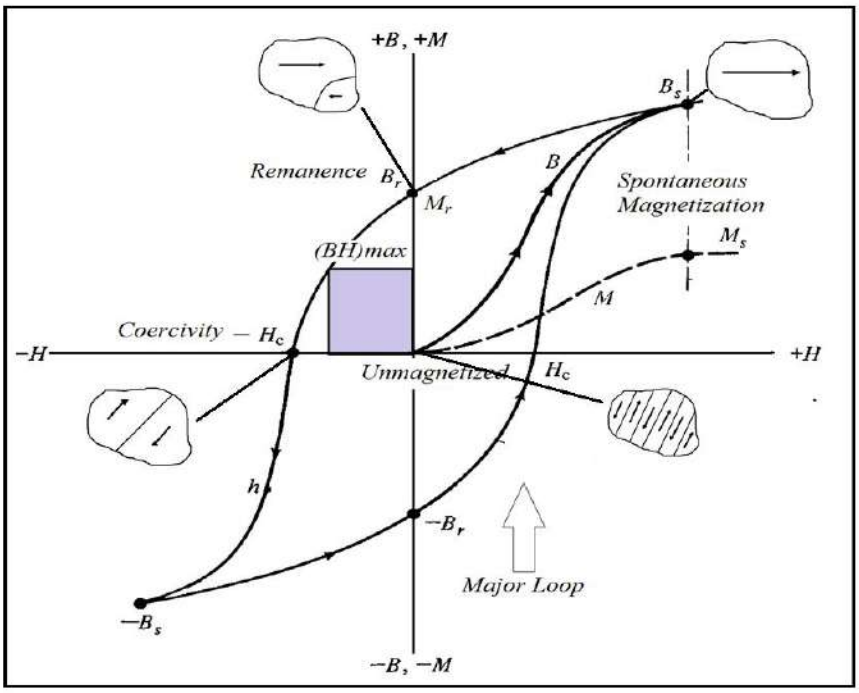

Figure: Hysteresis Curve for a Ferromagnetic Material showing the magnetic domain structure at different stages during magnetization process

Coercive field, H_c, is defined as the intensity of the applied magnetic field along the negative axes which is required to reduce the magnetization of the material to zero after it has reached its saturation. After applying a high enough reversal field, again, the saturation magnetization will be achieved in the negative direction. If the negative applied field is then decreased and again applied in the positive direction then the full hysteresis loop is obtained as shown in the figure 1.5. The area under the hysteresis loop indicates the amount of energy absorbed by the magnetic material during each cycle of the loop. [6]

When we apply smaller maximum field in either direction of a ferromagnetic sample, we do not get fully saturated sample and a minor loop is achieved. Minor loops usually are avoided since the size of the loop depends on the maximum field supplied and not solely on the magnetic properties of the sample.

The **maximum energy product $(BH)_{max}$** is energy stored in the magnet and it given by the maximum rectangular area inscribed under the B(H) curve. It measures the value of maximum

amount of useful work that can be done by the permanent magnet. The product $(BH)_{max}$ tends to increase with increase in both of the coercive field, H_c and saturation magnetization, M_s.

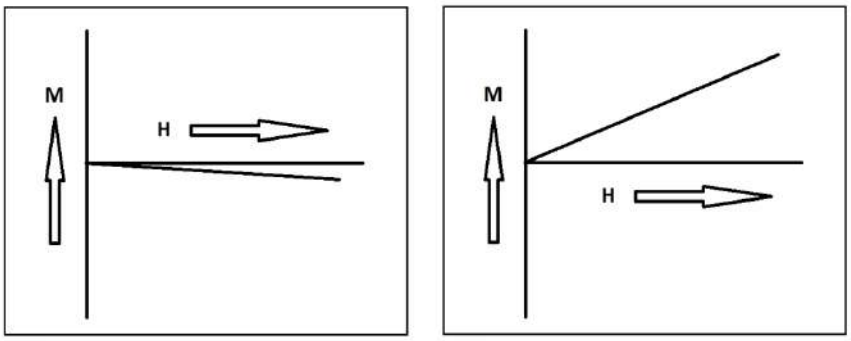

Figure: M-H plots for (a) Diamagnetism (b) paramagnetism

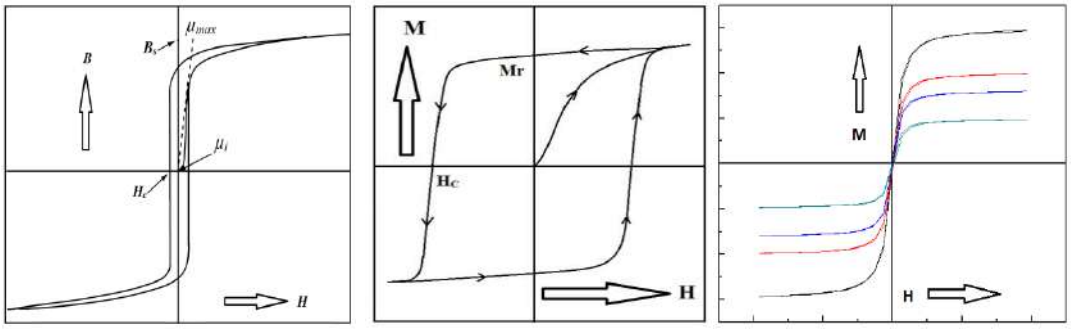

Figure: Hysteresis curves for (a) soft magnets (b) hard magnets (c) ferrimagnets (4 samples)

Vibrating Sample Magnometer (VSM)

Vibrating sample magnetometer (VSM) is one of the most important scientific device which is commonly used in determination of different types of magnetic properties of all types of magnetic materials paramagnetic, ferromagnetic, diamagnetic, anti-ferromagnetic, high and low temperature superconducting and magnetic optical materials etc. This scientific device was invented by Simen Foner in 1955. A great number of modifications have been made in the first model of vibrating sample magnetometer to avail the efficient use of this instrument.

Principal

Vibrating sample magnetometer works on the basis of Faraday law of electromagnetic induction. According to this law induced voltage in the coil is directly proportional to the rate of change of flux in the coils. Mathematical form of Faraday law is given below.

$$V = -N\frac{d\emptyset}{dt}$$

Where "N" is the number of turns of the coil, "ϕ" is the magnetic flux which is passing through the coil and "dϕ/dt" is the rate of the change of magnetic flux. Flux density B can be found as ϕ = B.A. So,

$$V = -NA\frac{dB}{dt}$$

According to the equation above we can easily calculate the flux density "B" by measuring the induced voltage in the coils. Block diagram of vibrating sample magnetometer is shown in Figure.

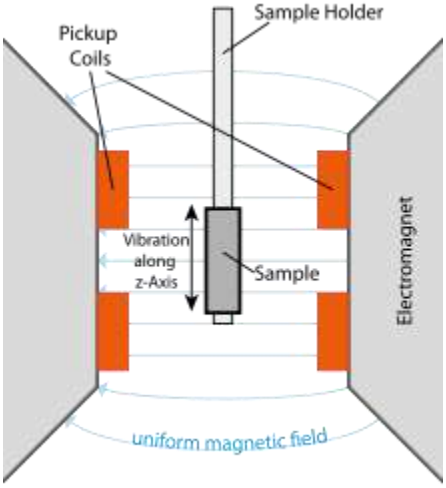

Block diagram of Vibrating Sample Magnetometer

Construction of Vibrating Sample Magnetometer

There are different parts of vibrating sample magnetometer which are given below.

- Sensor coil
- Water cool electromagnet
- Vibration exciter
- Sample holder
- Hall probe
- Amplifier

- Control chassis
- Lock in amplifier
- Power supply
- Computer interface

Facilities Available in VSM

Easy Sample Exchange: The sliding head mechanism allows easy sample exchange and positioning, ensuring reproducibility of measured results

Multiple Magnet Configurations: 100 mm, 175 mm, and 250 mm (4 in, 7 in, and 10 in) variable-gap electromagnet-based configurations provide fields to 3.1 T

Sample Holders: Accommodate thin film, bulk, liquid, and powder samples

Variable Temperature: Measure samples from -269 °C to 1000 °C (4.2 K to 1273 K) with our variable temperature options and the broadest temperature range of any electromagnet-based VSM

Anisotropy Measurements: Vector coil and autorotation options enable investigations of magnetically anisotropic materials, including derived torque curves

Magnetoresistance Probe: Perform fast and accurate magnetoresistance measurements with this option as a function of both magnetic field and temperature

Helmholtz Coil: An option for applications requiring measurements at fields less than 8 kA/m (100 Oe)

Integrated Software: Set up and execute measurement routines and experiments quickly and easily from the Windows® menu-driven interface

Detailed Post Processing: Background corrections, automatic offset removal, derivative curves, parameter extraction, and more

Working of Vibrating Sample Magentometer (VSM)

When sample is placed in the electromagnets of VSM which can produce magnetic field upto 9 tesla, so an induced magnetic moment is produce in the sample which can be measured by the sensor coils. These coils evaluated induced magnetic moment which allocated symmetrically on sample along the axis of detection coils to the magnetic field. Sample become magnetized, it vibrated back and forth with small oscillations. These oscillations are the source of time varying magnetic flux, which induced an electromotive force (emf) in coil which according to the Faraday's law of electromagnetic induction because magnitude of induced emf is directly proportional to the total magnetic moment of the sample. So we get B-H loop or M-H loop by gradually sweeping of applied negative field. By the help of VSM we can measure hysteresis loop of every type of sample such as thin films or bulk sample.

Figure 3.16: Lake Shore 7470 VSM at Centre excellence in solid state physics

Purposes of VSM

The following parameters are either measured directly or can easily be derived through the software

- Hysteresis Loops: Saturation magnetization (M_S), Retentivity or remanent magnetization (M_R), Coercivity (H_c), Intrinsic coercivity (H_{ci}), Slope and differential susceptibility at H_c,
- Switching field distribution (SFD)
- Flatness,
- Squareness ratio (SQR)

- Minor hysteresis loops
- Initial magnetization curve
- AC remanence
- Magnetic Moment as a function of pressure: VSM is used as non-magnetic high hydrostatic pressure clamp device.
- Magnetization vs. Temperature
- Magnetization vs. Time
- DC Demagnetization
- IRM (Irreversible Remnant Magnetization)
- 2nd quadrant demagnetization curves Maximum energy Product (BHMAX)
- Isothermal (IRM) remanence Permeability curves
- Magnetic anisotropy
- Curie point
- Magnetic viscosity

Materials Used

All types of magnetic materials:

- Diamagnetic, Paramagnetic, Ferromagnetic, Ferrimagnetic, Antiferromagnetic materials and Anisotropic materials
- Particulate and continuous magnetic recording materials and GMR, CMR, exchange biased and spin-valve materials
- Magnetic-optical materials
- Bulk materials, powders, thin films, single crystals, and liquids are readily accommodated

Features

- Computer-automated data collection system providing field strengths to 23 kG
- Measurement of moments as small as 0.1×10^{-6} emu in room temperature magnetic fields ranging from -23 to +23 kG

- Adjustable magnet air gap permits adjusting magnet/coils to suit sample and field strength requirements
- Bipolar power supply provides smooth continuous transition through zero field
- Fast data acquisition - average sample run (hysteresis loop) over full field range typically requires only minutes
- Windows™ NT/2000 menu driven color graphic software for system operation, data acquisition, and analysis. System software includes operation and control of the magnet power supply, VSM control unit, and gaussmeter. Real-time feedback of processed magnetic moment measurement data can be displayed in either graphical or tabular format.
- Water cooled magnet coils provide excellent field stability when high power is required to achieve the maximum field capability

Spectroscopic Ellipsometery

Spectroscopic ellipsometry is a sensitive and non-destructive technique to determine the optical properties such as refractive index, extinction coefficient, band gap energy etc. of thin film. It is used to measure the accurate thickness of the film, thickness determinations ranging from a few angstroms to tens of microns are possible for single layers and complex multilayer stacks.
When the light from a particular angle is incident on the surface of the film, linearly polarized light is reflected in elliptical shape. The size, orientation and shape of the ellipse depend upon the reflection properties of the surface of the sample, angle of incidence, the direction of polarization of incident light. One can determine the polarization of reflected light with the help of quarter-wave plate followed by an analyzer. The direction of the quarter-wave plate and analyzer are changed until no reflected light passes through the analyzer. From these orientations of polarization of the incident light one can determine the relative amplitude (ψ) and relative phase change (Δ). The reflection property of the surface is changed, depending upon roughness or smoothness of the film surface. After measuring these changes in the reflection properties one can determine the actual change in the films thickness.

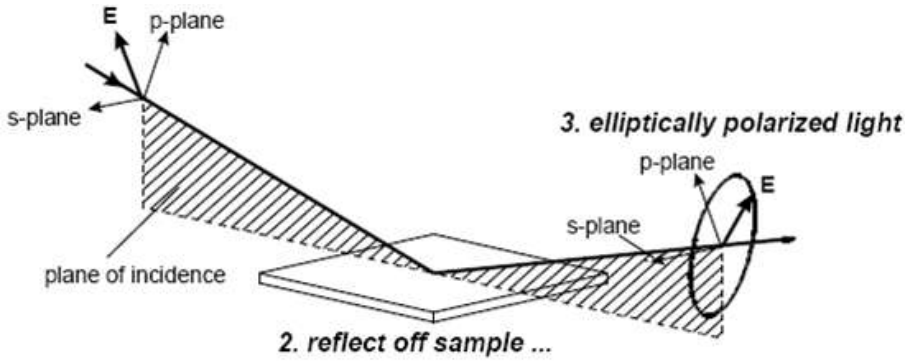

Figure: Interaction of polarized light with sample

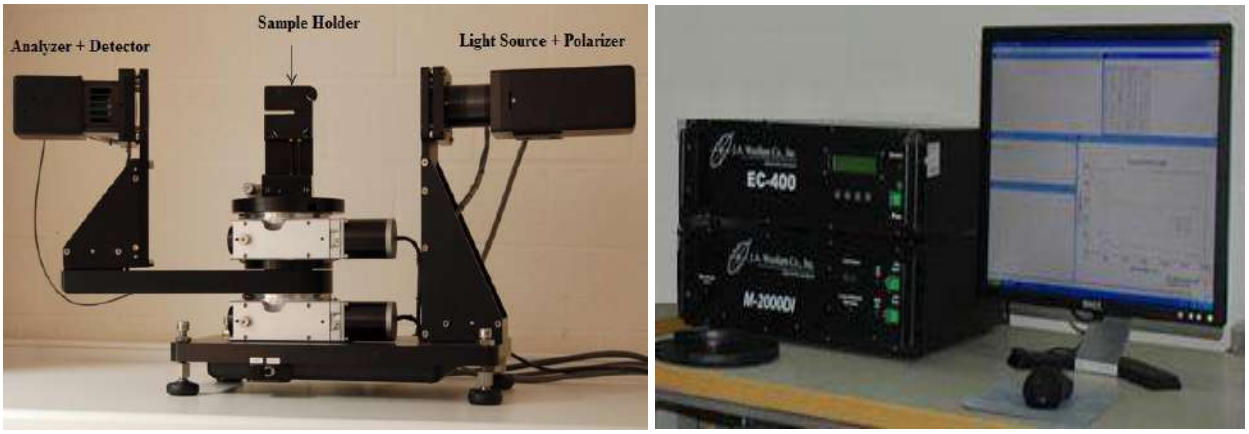

Spectroscopic Ellipsometer with Control Panel

Spectroscopic ellipsometer could measure the thickness of the thin films by using the interference data calculated from the reflected beam. Actually the phase variation of the incident light occurs during the reflection from the film surface and substrate surface as shown in figure. These phase variations are related to thickness of thin film and cause constructive and destructive interference patterns.

Interaction of Light and Ellipsometry Measurements

When light proceeds from one medium into another (e.g., from air into a solid substance), several things happen. Some of the light radiation may be transmitted through the medium, some will be absorbed, and some will be reflected at the interface between the two media. The intensity of the beam incident to the surface of the solid medium must equal the sum of the intensities of the transmitted, absorbed, and reflected beams, denoted as and respectively, or

$$I_O = I_T + I_A + I_R$$

Radiation intensity, expressed in watts per square meter, corresponds to the energy being transmitted per unit of time across a unit area that is perpendicular to the direction of propagation. An alternate form of above equation is

$$T + A + R = 1$$

where T, A, and R represent, respectively, the transmissivity (I_T/I_0), absorptivity (I_A/I_0) and reflectivity (I_R/I_0) or the fractions of incident light that are transmitted, absorbed, and reflected beams; absorbed, and reflected by a material; their sum must equal unity, since all the incident light is either transmitted, absorbed, or reflected.

Materials those are capable of transmitting light with relatively little absorption and reflection are **transparent -** one can see through them. **Translucent** materials are those through which light is transmitted diffusely; that is, light is scattered within the interior, to the degree that objects are not clearly distinguishable when viewed through a specimen of the material. Materials that are impervious to the transmission of visible light are termed **opaque**. Bulk metals are opaque throughout the entire visible spectrum; that is, all light radiation is either absorbed or reflected. On the other hand, electrically insulating materials can be made to be transparent. Furthermore, some semiconducting materials are transparent whereas others are opaque.

Refraction: Light that is transmitted into the interior of transparent materials experiences a decrease in velocity, and, as a result, is bent at the interface; this phenomenon is termed refraction. The **index of refraction** n of a material is defined as the ratio of the velocity in a vacuum c to the velocity in the medium. The magnitude of n (or the degree of bending) will depend on the wavelength of the light. This effect is graphically demonstrated by the familiar dispersion or separation of a beam of white light into its component colors by a glass prism. Not only does the index of refraction affect the optical path of light, but also, as explained below, it influences the fraction of incident light that is reflected at the surface. Refractive index is given:

$$n = \frac{c}{v} = \frac{\sqrt{\epsilon\mu}}{\sqrt{\epsilon_0 \mu_0}} = \sqrt{\epsilon_r \mu_r}$$

Where ε_r and μ_r are the dielectric constant and the relative magnetic permeability of the substance under observation, respectively. Since most substances are only slightly magnetic, so,

$$n \cong \sqrt{\epsilon_r}$$

Thus, for transparent materials, there is a relation between the index of refraction and the dielectric constant. The phenomenon of refraction is related to electronic polarization at the relatively high frequencies for visible light; thus, the electronic component of the dielectric constant may be determined from index of refraction measurements using above equation.

Since the retardation of electromagnetic radiation in medium results from electronic polarization, the size of the constituent atoms or ions has a considerable influence on the magnitude of this effect- generally, the larger an atom or ion, the greater will be the electronic polarization, the slower the velocity, and the greater the index of refraction. The index of refraction for a typical soda–lime glass is approximately 1.5. *Additions of large barium and lead ions (as BaO and PbO) to a glass will increase n significantly*. For crystalline ceramics that have cubic crystal structures, and for glasses, the index of refraction is independent of crystallographic direction

(i.e., it is isotropic). Noncubic crystals, on the other hand, have an anisotropic n; that is, the index is greatest along the directions that have the highest density of ions.

Reflection: The reflectivity R represents the fraction of the incident light that is reflected at the interface,

$$R = \left(\frac{n_2 - n_1}{n_2 + n_1}\right)^2$$

where n_1 and n_2 are the indices of refraction of the two media. If the incident light is not normal to the interface, R will depend on the angle of incidence. When light is transmitted from a vacuum or air into a solid s, then

$$R = \left(\frac{n_s - 1}{n_s + 1}\right)^2$$

since the index of refraction of air is very nearly unity. Thus, the higher the index of refraction of the solid, the greater is the reflectivity. Just as the index of refraction of a solid depends on the wavelength of the incident light, so also does the reflectivity vary with wavelength. Reflection losses for lenses and other optical instruments are minimized significantly by coating the reflecting surface with very thin layers of dielectric materials.

Absorption: Light radiations are absorbed in the materials by two basic mechanisms: electronic polarization and valence band-conduction band electron transitions. Absorption by electronic polarization is important only at light frequencies in the vicinity of the relaxation frequency of the constituent atoms. The valence band-conduction band electron transitions depend on the electron energy band structure of the material. Absorption of a photon of light may occur by the promotion or excitation of an electron from the nearly filled valence band, across the band gap, and into an empty state within the conduction band.

These excitations with the accompanying absorption can take place only if the photon energy is greater than that of the band gap - that is, if

$$h\nu > E_g \qquad \frac{hc}{\lambda} > E_g$$

From the minimum and maximum wavelength for visible light, values for the maximum band gap energy (3.1 eV) and the minimum band gap energy (1.8 eV) can be calculated for which absorption of visible light is possible. No visible light is absorbed by non-metallic materials

having band gap energies greater than about 3.1 eV; these materials, if of high purity, will appear transparent and colorless. On the other hand, all visible light is absorbed by valence band-to-conduction band electron transitions for those semiconducting materials that have band gap energies less than about 1.8 eV; thus, these materials are opaque. Only a portion of the visible spectrum is absorbed by materials having band gap between 1.8 and 3.1 eV; consequently, these materials appear colored. Thus

- If $E_{gap} < 1.8$ eV, full absorption; color is black (Si, GaAs)
- If $E_{gap} > 3.1$ eV, no absorption; colorless (diamond)
- If E_{gap} in between, partial absorption; material has a color

Interactions with light radiation can also occur in dielectric materials having wide band gaps, involving impurities or other electrically active defects are present. Electron levels within the band gap may be introduced, such as the donor and acceptor levels. Light radiation of specific wavelengths may be emitted as a result of electron transitions involving these levels within the band gap.

The intensity of the net absorbed radiation is dependent on the character of the medium as well as the path length within. The intensity of transmitted or non-absorbed radiation continuously decreases with distance x that the light traverses:

$$I'_T = I'_0 e^{-\beta x}$$

where the absorption coefficient varies with wavelength of the incident radiation. The distance parameter x is measured from the incident surface into the material. Materials that have large values of β are considered to be highly absorptive and β is related to the transmission:

$$\beta = -\frac{1}{x} \ln T$$

Transmission: The phenomena of absorption, reflection, and transmission may be applied to the passage of light through a transparent solid. For an incident beam of intensity I_0 that impinges on the front surface of a specimen of thickness *l* and absorption coefficient, β, the transmitted intensity I_T at the back face is

$$I_T = I_0(1 - R)^2 e^{-\beta l}$$

where R is the reflectance; it is assumed that the same medium exists outside both front and back faces. Thus, the fraction of incident light that is transmitted through a transparent material depends on the losses that are incurred by absorption and reflection.

Ellipsometry uses polarized light to characterize thin film and bulk materials. The light undergoes a change in polarization as it interacts with the sample structure. The measurement is typically expressed as two values: **Psi (Ψ) and Delta (Δ).** Psi (Ψ) and Delta (Δ) represent the raw measurement from an ellipsometer. They describe the change in polarization that occurs when the measurement beam interacts with a sample surface. The incident light beam contains electric fields both parallel (p-) and perpendicular (s-) to the plane of incidence. The data are then analyzed to determine material properties of interest.

The surface of the sample differentiates between the p- and s- light, causing a change in the outgoing polarization. This is represented by both an amplitude ratio (tanΨ) and phase difference (Δ):

$$\tan(\Psi)\ e^{i\Delta} = \frac{R_P}{R_S}$$

where Rp and Rs are the Fresnel reflection coefficients for the p- and s- polarized light, respectively. We can determine film thickness, optical constants, refractive index, surface roughness, and other physical properties of the sample. These properties are found by using the measured values of (Ψ and Δ) in various equations and algorithms to produce a model that describes the interaction of light with the sample. A specific wavelength range is often required to measure special material properties because for many applications, optical properties are desired at specific wavelengths.

Spectroscopic ellipsometry is very sensitive to the **film thickness**. As the film thickness increases, there is an increasing separation between the light reflected from the surface and the light that travels through the film. This causes a phase delay that is related to both the physical thickness and the index of refraction. Thus, spectroscopic ellipsometry measurements contain the information to accurately measure both thickness and index. It provides information about the thickness based on the position and number of interference oscillations. As the thickness increases, the interference oscillations shift toward longer wavelengths. While the index of refraction will be wavelength dependent, the thickness remains the same.

Spectroscopic ellipsometry can measure the thickness of the order of just a fraction of a nanometer. The upper thickness limit for spectroscopic ellipsometry measurements depends on the measurement wavelengths. As the film becomes thicker, the large number of data oscillations becomes difficult to resolve at shorter wavelengths. The oscillations are better separated at longer wavelengths. Thus, it is common to use near infrared or even mid-infrared measurements to measure films up to 50 microns thick. However, these layers are beyond the typical range for SE measurements, and film uniformity becomes much more important. The preferred limit for most visible-to-near infrared measurements is less than 5 microns. Even for films that are 1 to 5

microns thick, it is best to measure with multiple angles of incidence to gain confidence that you have a unique thickness solution. In addition to thickness information, the shape of the data oscillations is dependent on the film index of refraction. The amplitude of the oscillations determines the correct refractive index of the film.

$$\tilde{n} = n + i\kappa.$$
$$k = \frac{2\pi n}{\lambda_0}$$
$$\alpha = \frac{4\pi\kappa}{\lambda_0}$$

where $\tilde{n}$ is the **complex refractive index**. Here, the **real part of the refractive index n** indicates the phase velocity, while the imaginary part κ indicates the amount of absorption loss when the electromagnetic wave propagates through the material and is known as the **extinction coefficient**. λ_o is the wavelength of the inccident light. α is the **absorption coefficient** and it is related to the penetration depth, the distance after which the intensity is reduced by 1/e, $\delta_p = \frac{1}{\alpha} = \frac{\lambda_0}{4\pi\kappa}$.

$$\mathrm{OPL} = nd$$

Optical path length (OPL) is the product of the geometric length d of the path light follows through a system, and the index of refraction of the medium through which it propagates.

Complex dielectric constant in term of refractive index and extinction coefficient is

$$\tilde{\epsilon} = \epsilon_1 + i\epsilon_2 = (n + i\kappa)^2.$$

Conversion between refractive index and dielectric constant is done by:

$$\epsilon_1 = n^2 - \kappa^2$$
$$\epsilon_2 = 2n\kappa$$
$$n = \sqrt{\frac{\sqrt{\epsilon_1^2 + \epsilon_2^2} + \epsilon_1}{2}}$$
$$\kappa = \sqrt{\frac{\sqrt{\epsilon_1^2 + \epsilon_2^2} - \epsilon_1}{2}}.$$ [33]

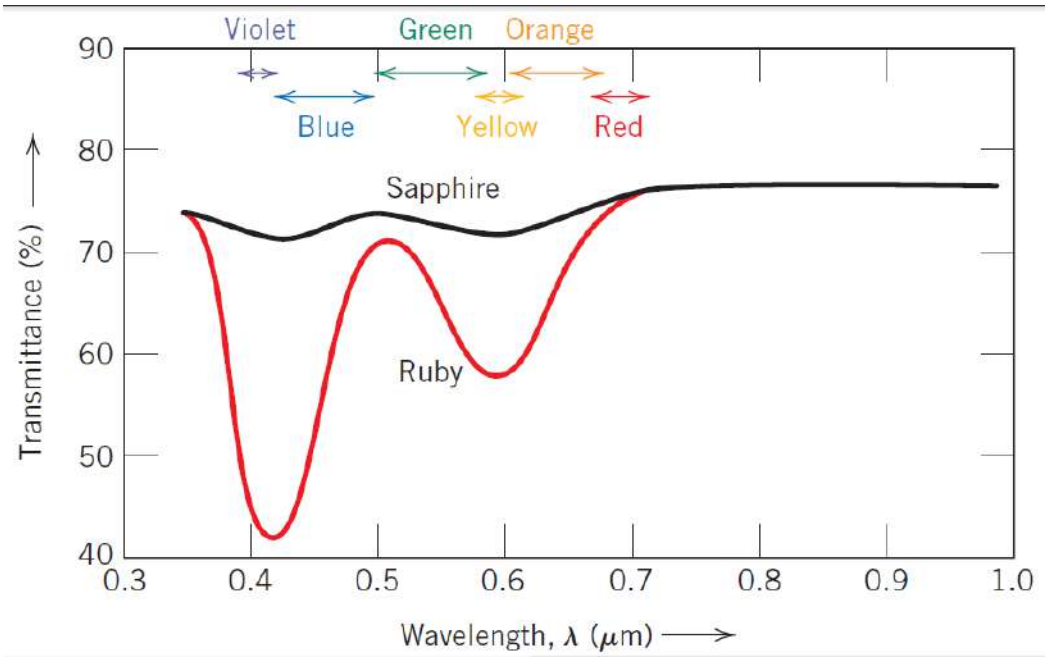

Above figure shows transmission of light radiation as a function of wavelength for sapphire (single-crystal aluminum oxide) and ruby (aluminum oxide containing some chromium oxide).

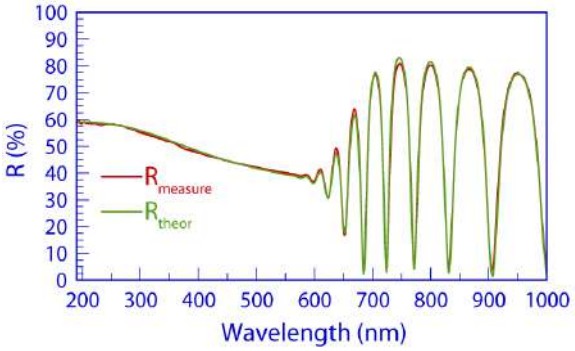

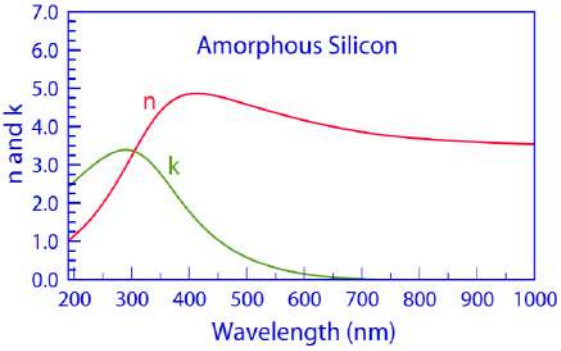

Above figure shows reflectance spectra collected over 190nm-1000nm wavelength range for an amorphous silicon film on an oxidized silicon substrate plus the n(λ) and k(λ) spectra of the film. The film thickness was found to be 1147nm.

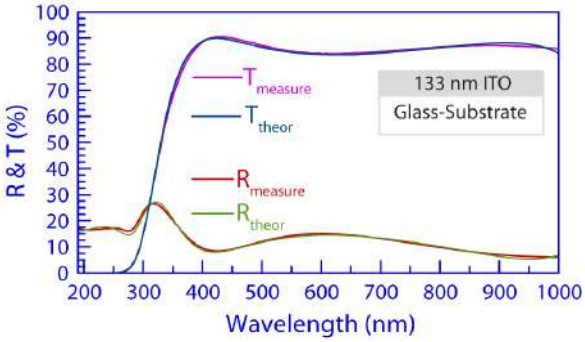

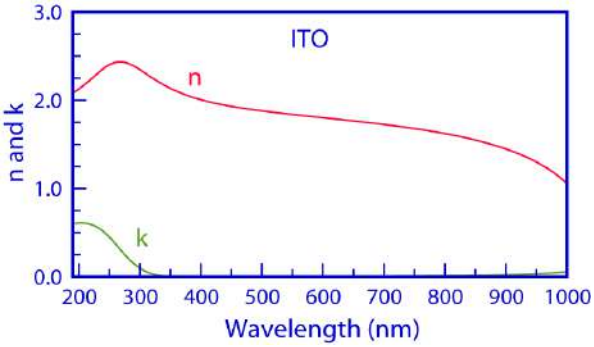

Above figures show that reflectance and transmittance spectra from 190nm - 1000nm of ITO deposited on the glass substrate described above, plus the n(λ) and k(λ) spectra of the ITO film. ITO thickness of 133nm and its n(λ) and k(λ) spectra were simultaneously determined .

Fourier Transform Infrared Spectroscopy (FTIR)

Fourier transform infrared spectroscopy (FTIR) is a technique which is used to obtain an infrared spectrum of absorption, emission, photoconductivity or Raman scattering of a solid, liquid or gas. An FTIR spectrometer simultaneously collects spectral data in a wide spectral range. FTIR is the preferred method of infrared spectroscopy. Like a fingerprint no two unique molecular structures produce the same infrared spectrum. This makes infrared spectroscopy useful for several types of analysis.

Advantages

- It can identify unknown materials
- It can determine the quality or consistency of a sample
- It can determine the amount of components in a mixture

Fourier transform infrared spectroscopy is preferred over dispersive or filter methods of infrared spectral analysis for several reasons:

- It is a non-destructive technique
- It provides a precise measurement method which requires no external calibration
- It can increase speed because all of the frequencies are measured simultaneously
- It can increase sensitivity because the detectors employed are much more sensitive and fast and with much lower noise levels
- It is mechanically simple with only one moving mirror in the interferometer
- These instruments employ a HeNe laser as an internal wavelength internal calibration standard.

Thus, it is a very reliable technique for positive identification of virtually any sample. In addition, the sensitivity and accuracy of FTIR detectors, along with a wide variety of software algorithms, have dramatically increased the practical use of infrared for quantitative analysis.

Qualitative Analysis of Materials

Infrared spectrum represents a fingerprint of a sample with absorption peaks which correspond to the frequencies of vibrations between the bonds of the atoms making up the material. Because each different material is a unique combination of atoms, no two compounds produce the exact same infrared spectrum. Therefore, infrared spectroscopy can result in a positive identification (qualitative analysis) of every different kind of material. In addition, the size of the peaks in the spectrum is a direct indication of the amount of material present. With modern software algorithms, infrared is an excellent tool for quantitative analysis.

Construction and Working

The normal instrumental process is as follows:

The Source: Infrared energy is emitted from a glowing black-body source. This beam passes through an aperture which controls the amount of energy presented to the sample (and, ultimately, to the detector).

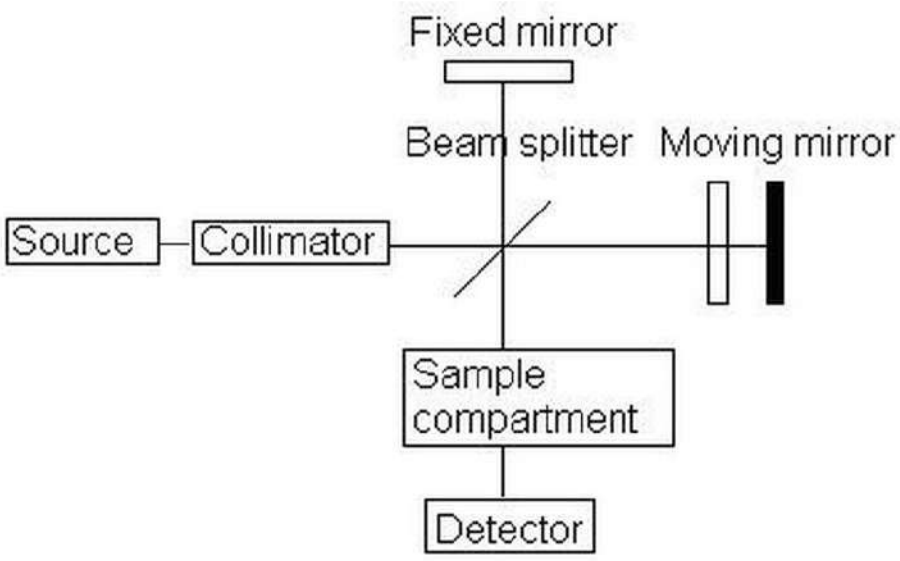

Block diagram of an FTIR spectrometer

The Interferometer: The beam enters the interferometer where the “spectral encoding” takes place. The resulting interferogram signal then exits the interferometer.

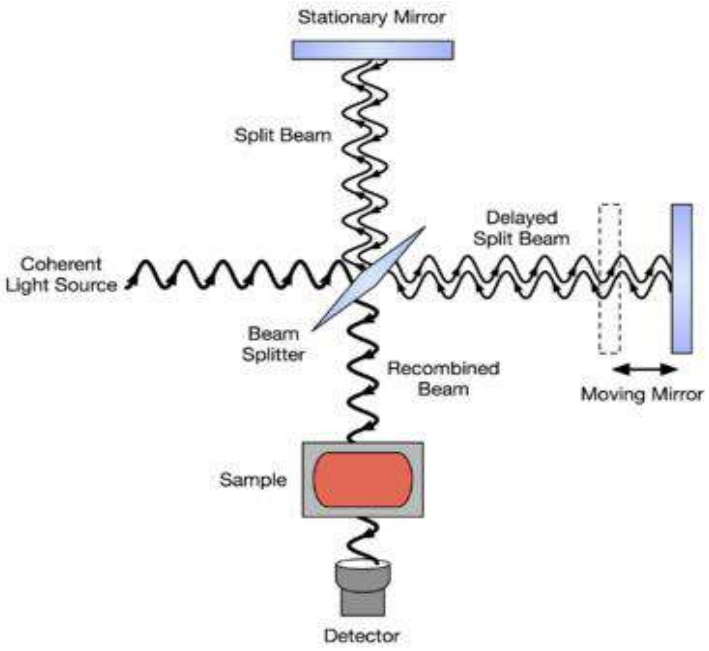

The Sample: The beam enters the sample compartment where it is transmitted through or reflected off of the surface of the sample, depending on the type of analysis being accomplished. This is where specific frequencies of energy, which are uniquely characteristic of the sample, are absorbed.

The Detector: The beam finally passes to the detector for final measurement. The detectors used are specially designed to measure the special interferogram signal.

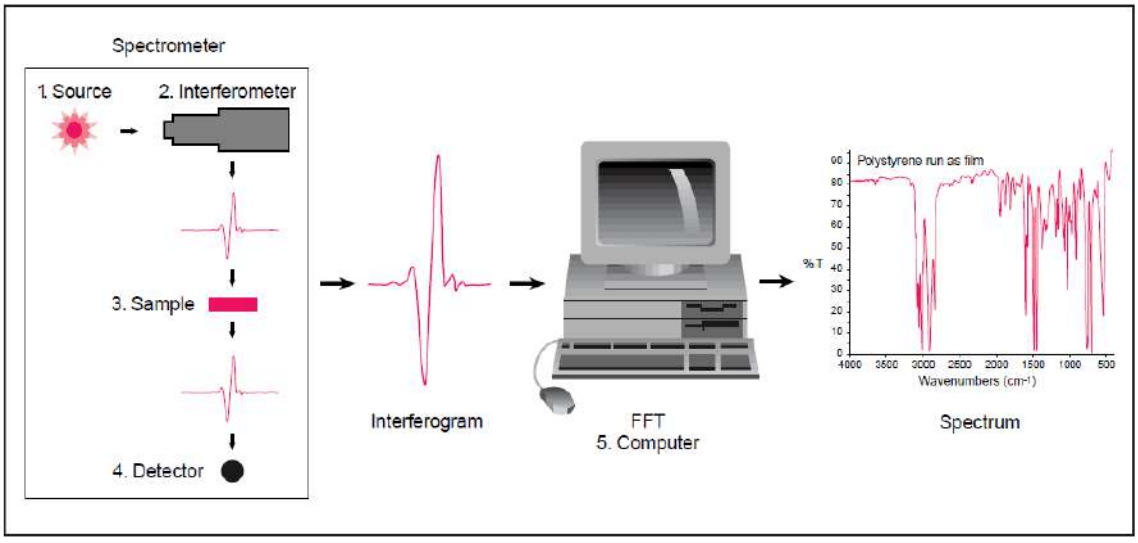

The Computer: The measured signal is digitized and sent to the computer where the Fourier transformation takes place. The final infrared spectrum is then presented to the user for interpretation and any further manipulation.

Because there needs to be a relative scale for the absorption intensity, a background spectrum must also be measured. This is normally a measurement with no sample in the beam. This can be compared to the measurement with the sample in the beam to determine the "percent transmittance." This technique results in a spectrum which has all of the instrumental characteristics removed. Thus, all spectral features which are present are strictly due to the sample. A single background measurement can be used for many sample measurements because this spectrum is characteristic of the instrument itself.

Fourier Transform Infrared (FTIR) Spectrometry was developed in order to overcome the limitations encountered with dispersive instruments. The main difficulty was the slow scanning process. A method for measuring all of the infrared frequencies simultaneously, rather than individually, was needed. A solution was developed which employed a very simple optical device called an interferometer. The interferometer produces a unique type of signal which has all of the infrared frequencies "encoded" into it. The signal can be measured very quickly, usually on the order of one second or so. Thus, the time element per sample is reduced to a matter of a few seconds rather than several minutes.

Most interferometers employ a beamsplitter which takes the incoming infrared beam and divides it into two optical beams. One beam reflects off of a flat mirror which is fixed in place. The other beam reflects off of a flat mirror which is on a mechanism which allows this mirror to move a very short distance (typically a few millimeters) away from the beamsplitter. The two beams reflect off of their respective mirrors and are recombined when they meet back at the beamsplitter. Because the path that one beam travels is a fixed length and the other is constantly changing as its mirror moves, the signal which exits the interferometer is the result of these two beams "interfering" with each other. The resulting signal is called an interferogram which has the unique property that every data point (a function of the moving mirror position) which makes up the signal has information about every infrared frequency which comes from the source.

This means that as the interferogram is measured, all frequencies are being measured simultaneously. Thus, the use of the interferometer results in extremely fast measurements. Because the analyst requires a frequency spectrum (a plot of the intensity at each individual frequency) in order to make identification, the measured interferogram signal cannot be interpreted directly. A means of "decoding" the individual frequencies is required. This can be accomplished via a well-known mathematical technique called the Fourier transformation. This transformation is performed by the computer which then presents the user with the desired spectral information for analysis.

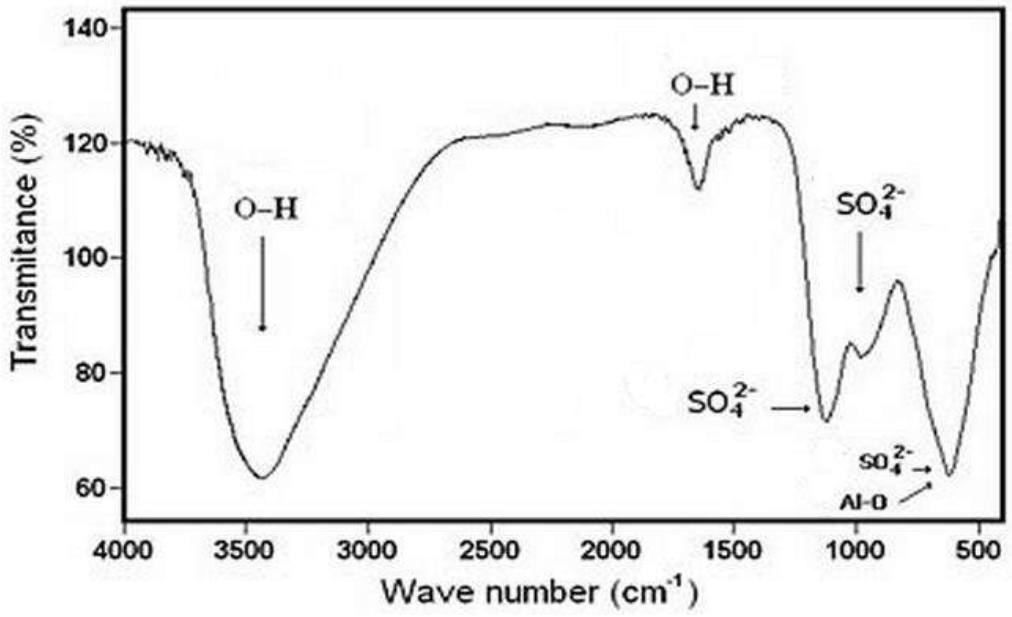

The FTIR spectrum of basic aluminum sulphate is shown in figure. It shows the broad O-H stretching band in the 3000 to 3700 cm^{-1} range and the absorption band which peaks at 1655 cm^{-1}, indicating that the solid is a hydrate. The strong and broad band centered at 1135 cm^{-1} and the small shoulder at 998 cm^{-1} could be assigned to sulfate absorptions. The strong and broad absorption band centered at 613 cm^{-1} probably resulted from the combined absorptions of sulfate, the Al-O stretching vibrations and the Al-OH wagging vibrational mode of molecular water. Therefore, this compound corresponded to a hydrated basic aluminum sulfate.

Electrical Measurements:

Electrical resistivity is also known as specific electrical resistance. It measures the opposition which "material" shows to the flow of current. A low resistivity indicates that material allows the easy flow of current.

- Conductors have very low resistivity 10^{-2} Ωm.
- Semiconductors have intermediate resistivity 10^{2} Ωm.
- Insulators have very high resistivity 10^{6}-10^{12} Ωm.

Van Der Pauw method (4 Probe-Method)

The van der Pauw Method is a technique commonly used to measure the resistivity and the Hall coefficient of a sample. Its power lies in its ability to accurately measure the properties of a sample of any arbitrary shape, so long as the sample is approximately two-dimensional (i.e. it is much thinner than it is wide), solid and the electrodes are placed on its perimeter. With the help of Van Der Pauw methods, **we can measure**:

- The resistivity of the material at different temperatures
- The doping type (i.e. whether it is a P-type or N-type material)
- The sheet carrier density of the majority carrier
- The mobility of the majority carrier
- Determination of the Band-gap

Before characterization these **conditions** must be satisfied to use this technique:

1. The sample must have a flat shape of uniform thickness
2. The sample thickness must be much less than the width and length of the sample
3. The sample must not have any isolated holes
4. The sample must be homogeneous and isotropic
5. All four contacts must be located at the edges of the sample

6. The area of contact of any individual contact should be at least an order of magnitude smaller than the area of the entire sample.

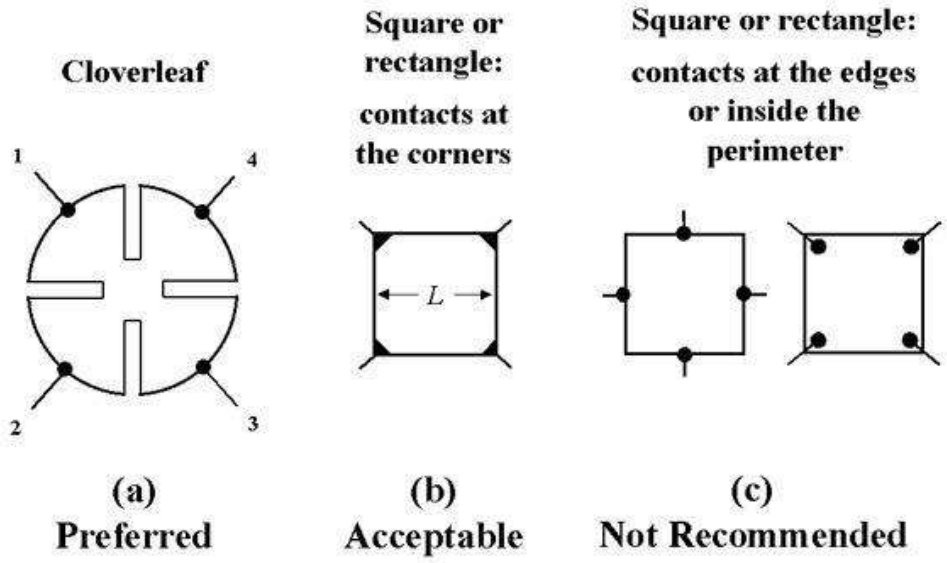

Figure: Possible Arrangements for ohmic contacts

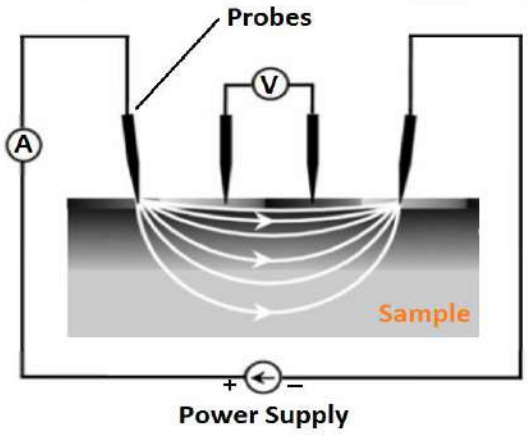

Figure: Schematic Diagram for Four Probe Method

Figure: Four Probe Set-up

The measurements require that four ohmic contacts be placed on the sample. Certain conditions for their placement need to be met:

- Contacts must be on the boundary of the sample.
- Contacts must be infinitely small. Practically, they must be as small as possible.

Measurement Arrangements: A sample holder equipped with two electrodes made up of copper was used for the resistivity measurement. A sensitive electrometer and dc power supply was connected in series with the sample holder. Current can be measured by varying the voltage from power supply. The contacts are numbered from 1 to 4 in a counter-clockwise order.
The current I_{12} is applied across contact 1 and contact 2, and the voltage V_{34} is measured between contacts 3 and 4 with no externally applied magnetic field. From these two values, a resistance (for this example, $R_{12,34}$) can be found using Ohm's law:

$$R_{12,34} = \frac{V_{34}}{I_{12}}$$

Van der Pauw showed that the sheet resistance of samples with arbitrary shapes can be determined from two of these resistances - one measured along a vertical edge, such as $R_{12,34}$, and a corresponding one measured along a horizontal edge, such as $R_{23,41}$ where

$$R_{23,41} = \frac{V_{41}}{I_{23}}$$

The actual sheet resistance is related to these resistances by the van der Pauw formula

$$e^{-\pi R_{12,34}/R_s} + e^{-\pi R_{23,41}/R_s} = 1$$

When the samples are cut in square shapes, $R_{vertical} = R = R_{horizontal}$ and in this scenario the sheet resistance is given by

$$R_s = \frac{\pi R}{\ln 2}$$

After calculating sheet resistance R_s, the average resistivity of a sample is calculated as:

$$\rho = R_s \times t$$

$$\rho = \frac{\pi R}{\ln 2} \times t$$

The resistivity ρ is measured in ohms·metres (Ω·m) where t is the thickness of the sample that is measured in metres (m).

Hall Measurements

When a charged particle is placed in a magnetic field, it experiences a Lorentz force proportional to the strength of the field and the velocity at which it is traveling through it. This force is strongest when the direction of motion is perpendicular to the direction of the magnetic field; in this case the force

$$F_L = qvB$$

where q is the charge on the particle in coulombs, v the velocity it is traveling and B the strength of the magnetic field.

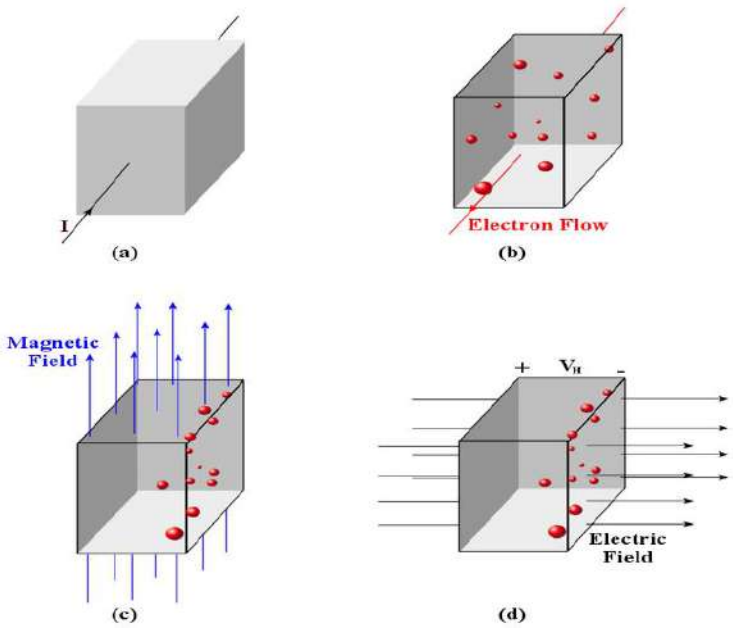

Figure: The Hall effect as it is used for the van der Pauw method. (a) current flowing through a piece of material (b) the electrons flowing due to the current (c) the electrons accumulating at one edge due to the magnetic field (d) the resulting electric field and Hall voltage due to accumulating electrons.

When a current is applied to a piece of semiconducting material this results in a steady flow of electrons through the material (as shown in figure). The velocity the electrons are traveling at is

$$v = \frac{I}{nAq}$$

where n is the electron density, A is the cross-sectional area of the material and q is the elementary charge.

If an external magnetic field is then applied perpendicular to the direction of current flow, then the resulting Lorentz force will cause the electrons to accumulate at one edge of the sample and given as:

$$F_L = \frac{IB}{nA}$$

This accumulation of electrons will create an electric field across the material due to the uneven distribution of charge. That in turn leads to a potential difference across the material, known as the Hall voltage V_H.

The current, however, continues to only flow along the material, which indicates that the force on the electrons due to the electric field balances the Lorentz force. Since the force on an electron from an electric field ϵ is $q\epsilon$, we can say that the strength of the electric field is therefore

$$\epsilon = \frac{IB}{qnA}$$

Finally, the magnitude of the Hall voltage is simply the strength of the electric field multiplied by the width of the material; that is,

$$V_H = w\epsilon$$

The polarity of this Hall voltage indicates the type of material the sample is made of; if it is positive, the material is P-type, and if it is negative, the material is N-type. The sheet density n_s is defined as the density of electrons multiplied by the depth of the material and can be calculated as:

$$n_s = \frac{IB}{q|V_H|}$$

Mobility

The resistivity of a semiconductor material can be shown to be

$$\rho = \frac{1}{q(n\mu_n + p\mu_p)}$$

where *n* and *p* are the concentration of electrons and holes in the material respectively, and μ_n and μ_p are the mobility of the electrons and holes respectively.

Generally, the material is sufficiently doped so that there is many orders-of-magnitude difference between the two concentrations, and so this equation can be simplified to

$$\rho = \frac{1}{qn_m\mu_m}$$

where n_m and μ_m are the doping level and mobility of the majority carrier respectively. Since

$$\rho = R_s \times t$$

$$R_s = \frac{\rho}{t}$$

By dividing the above equation by the thickness of the sample, we get the sheet resistance in terms of mobility:

$$R_s = \frac{1}{qn_s\mu_m}$$

This can then be rearranged to find the majority carrier mobility in terms of the previously calculated sheet resistance and sheet density:

$$\mu_m = \frac{1}{qn_sR_s}$$

Cancer Imaging and Inflammation Imaging

Cancer Imaging

Cancer may be difficult to detect, but for some types of cancer, the earlier it is detected, the better are the chances of treating it effectively. Imaging techniques - methods of producing pictures of the body - have become an important element of early detection for many cancers. But imaging is not simply used for detection.

Uses:

Cancer Imaging is important for determining the stage (telling how advanced the cancer is) and the precise locations of cancer to aid in directing surgery and other cancer treatments, or to check if a cancer has returned.

X-Ray Imaging

The most familiar use of X-rays is checking for broken bones, but X-rays are also used in cancer diagnosis.

- ✓ For example, chest radiographs and mammograms are often used for early cancer detection or to see if cancer has spread to the lungs or other areas in the chest.
- ✓ Mammograms use X-rays to look for tumors or suspicious areas in the breasts.

Uses:

- To diagnose early cancer

CT Scans

- ✓ A computed tomography scan (CT scan, also called a CAT scan) uses computer-controlled X-rays to create images of the body.
- ✓ However a radiograph and a CT scan show different types of information. Although an experienced radiologist can get a sense for the approximate three-dimensional location of a tumor from a radiograph, in general, a plain radiograph is two-dimensional.

Nuclear Imaging (PET and SPECT)

PET Scan

- The positron emission tomography (PET) scan creates computerized images of chemical changes, such as sugar metabolism, that take place in tissue.
- Typically, the patient is given an injection of a substance that consists of a combination of a sugar and a small amount of radioactively labeled sugar. The radioactive sugar can help in locating a tumor, because cancer cells take up or absorb sugar more avidly than other tissues in the body.

- After receiving the radioactive sugar, the patient lies still for about 60 minutes while the radioactively labeled sugar circulates throughout the body. If a tumor is present, the radioactive sugar will accumulate in the tumor. The patient then lies on a table, which gradually moves through the PET scanner 6 to 7 times during a 45-60-minute period.
- By the combined matching of a CT scan with PET images, there is an improved capacity to discriminate normal from abnormal tissues. A computer translates this information into the images that are interpreted by a radiologist.

Uses:

The PET scanner is used to detect the distribution of the sugar in the tumor and in the body.

SPECT Scan

- ✓ Similar to PET, single photon emission computed tomography (SPECT) uses radioactive tracers and a scanner to record data that a computer constructs into two- or three-dimensional images.
- ✓ A small amount of a radioactive drug is injected into a vein and a scanner is used to make detailed images of areas inside the body where the radioactive material is taken up by the cells.
- ✓ In this procedure, antibodies (proteins that recognize and stick to tumor cells) can be linked to a radioactive substance. If a tumor is present, the antibodies will stick to it. Then a SPECT scan can be done to detect the radioactive substance and reveal where the tumor is located.

Uses:

SPECT can give information about blood flow to tissues and chemical reactions (metabolism) in the body.

Ultrasound

Ultrasound image of the liver; dark areas by arrows show possible tumors.

Magnetic Resonance Imaging (MRI)

- Much like CT scans, MRI can produce three-dimensional images of sections of the body, but MRI is sometimes more sensitive than CT scans for distinguishing soft tissues.

Digital Mammography

Conventional mammography uses X-rays to look for tumors or suspicious areas in the breasts. Digital mammography also uses X-rays, but the data is collected on computer instead of on a piece of film.

Uses:

To presise location of tumors or suspicious areas in the breasts.

Virtual Colonoscopy

- ✓ Virtual colonoscopy (VC) (or Computerized Tomographic Colonography (CTC)) uses x rays and computers to produce two- and three-dimensional images of the colon (large intestine).
- ✓ VC can be performed with computed tomography (CT), sometimes called a CAT scan, or with magnetic resonance imaging (MRI).

Uses:

- Used to diagnose colon and bowel disease, including polyps, diverticulosis, and cancer.

Image-Guided Brain Surgery

This "hi-tech" involves conventional video image of a patient lying on the operating table is combined with MRI scans to locate key structural components of the brain and tumor. This allows the surgeon to see into the brain of a patient in a new way - virtually. Using this virtual image, the surgeon can make the best plan to enter the brain and remove the tumor, avoiding important brain structures and blood vessels.

- This new technology helps make brain surgery safer and less damaging.
- can help reduce the time spent in surgery
- reduce blood loss
- allows for removal of all the accessible tumor in one operation.

Inflammation Imaging

- ✓ The use of molecular imaging techniques allows the different components of the inflammatory response to be monitored *in situ* in humans.
- ✓ Acute and chronic lung diseases are almost invariably associated with some degree of inflammation.
- ✓ Inflammation imaging provides a unique tool for quantification of the modulation of discrete and specific aspects of inflammatory lung disease by targeted interventions. This should facilitate the development of new treatment strategies with better specificity for key elements of each disease.

Fluorodeoxyglucose positron emission tomography—computed tomography, or FDG-PET/CT,

- ✓ A highly sensitive imaging technique called fluorodeoxyglucose positron emission tomography—computed tomography, or FDG-PET/CT, which produces images that detect the metabolic activity of tissues within the body.
- ✓ FDG-PET/CT imaging is effective for identifying inflammation in the blood vessels, joints and liver, as well as the skin of patients with psoriasis who have not yet shown symptoms of problems in these areas.
- ✓ FDG-PET/CT can be used to detect inflammation in psoriasis and to understand if severe psoriasis affects critical organs beyond the skin.
- ✓ **Surgical Magnetic Systems and Tracers for Cancer Staging**
- ✓ Sentinel lymph node (SLN) biopsy is a minimally invasive alternative to routine axillary lymph node dissection, with few long-term side effects. Although numerous studies have demonstrated that SLN biopsy can accurately determine the axillary nodal status, the sensitivity of the procedure for detection of nodal metastases has been variable (seereviews in
- ✓ The most critical factor is the false-negative rate (the proportion of patients with axillary nodal metastases who are found, incorrectly, to have histologically negative SLNs). Although it has been suggested that a false-negative rate of approximately 5% is acceptable, false-negative rates from 10% to 19% have been reported in several series. Because of the variable false-negative rates and the fact that most of the published studies involve institutions and individuals specializing in breast cancer, there has been

skepticism about the ability to disseminate this technology into widespread surgical practice.

- ✓ A significant issue has been the lack of standardized methodology for the procedure. SLN biopsy is performed by mapping the lymphatic drainage after injection of a vital blue dye, radioactive colloid, or both around the breast tumor. The optimal technique is a subject of some controversy, and advocates of various techniques are divided roughly into three camps, comprising those who advocate the use of blue dye alone, radioactive colloid alone, or the combination of blue dye and radioactive colloid. The only previous large multi-institutional study, using radioactive colloid as a single agent, reported an 11.4% false-negative rate. The results of the present study indicate that, when applied in a multi-institutional setting, SLN biopsy using injection of both blue dye and radioactive colloid produces optimal results. The acceptable SLN identification and false-negative rates associated with the dual-agent injection technique indicate that this procedure is a suitable alternative to routine axillary dissection across a wide spectrum of surgical practice and hospital environments. There has been considerable controversy regarding theoptimal technique for SLN biopsy. Results of the present multi-institutional study indicate that injection of blue dye plus radioactive colloid injection provides more accurate nodal staging than the use of either agent alone. Although this is not a randomized study, the data support the use of the dual-agent injection as the method of choice to minimize false-negative results. These results do not, however, refute the excellent results obtained in some centers with single agent injection, but rather suggest that when SLN biopsy is performed across a wide range of surgical practices and hospital environments, the combination of blue dye plus radioactive colloid injection produces

more uniformly accurate nodal staging. Presumably, the combination of the two techniques— visualization of the blue dye and intra-operative gamma probe detection— provides overlapping and complementary ability to discriminate SLNs. This may be most helpful to

- ✓ surgeons and institutions with less experience in the technique. Although 72% of the SLNs in the dual-agent group were blue, the blue staining is often found only in retrospect after the radioactive node has been identified with the gamma probe. Alternatively, when a clear hot spot cannot be identified with the gamma probe, a blue lymphatic channel leading to a blue lymph node may be identified. The dual-agent injection technique was associated with a greater mean number of SLNs removed. The increased ability to identify multiple SLNs, when present, may account for the lower false-negative rate that was achieved using the dual agent injection technique In conclusion, the present study demonstrates that SLN biopsy can be performed with acceptable identification and false-negative rates across a wide variety of surgical practice and hospital environments if the combination of blue dye and radioactive colloid injection is used. Patient age and tumour location are important factors to take into account when discussing the possibilities of failure to identify the SLN or a false-negative SLN biopsy with patients. SLN biopsy is an acceptable alternative to axillary lymph node dissection for clinically node-negative breast cancer, provided that the surgeon and his or her hospital team demonstrate a low false-negative rate. Participation in ongoing clinical trials is strongly encouraged.

- ✓ Lymphatic System

- ✓ The lymphatic system is important to the body's defence mechanisms. It filters out organisms that cause disease, produces certain white blood cells and generates antibodies. It is also important for the distribution of fluids and nutrients in the body, because it drains excess fluids and protein so that tissues do not swell up. Lymph is a milky body fluid that contains a type of white blood cells, called lymphocytes, along with proteins and fats. Lymph seeps outside the blood vessels into the spaces of body tissues and is then stored in the lymphatic system to flow back into the bloodstream. Through the flow of blood in and out of arteries, and into the veins, and through the lymph nodes and into the lymph, the body is able to eliminate the products of cellular breakdown and bacterial invasion. It is through the actions of this system - which includes the spleen, the thymus, lymph nodes and lymph ducts - that our body is able to fight infection. Lymph plays an important role in the immune system and in absorbing fats from the intestines.

- ✓ The lymphatic vessels are present wherever there are blood vessels; they transport excess fluid to the end vessels without the assistance of any pumping action, such as is found in the cardiovascular system. There are more than 100 lymph nodes in the human body; these tiny, oval structures are mainly in the neck, groin and armpits, but there are several scattered all along the lymph vessels. They act as barriers to infection by filtering out and destroying toxins and germs. The largest body of lymphoid tissue in the human body is the spleen.

- ✓ Twenty-three patients with clinical submucosal thoracic squamous cell esophageal cancer were examined. Ferumoxides were injected endoscopically into the peritumoral submucosal layer, after which their appearance in the lymph nodes in the neck, superior mediastinum, and abdomen was evaluated using MRI.

- ✓ Magnetic multiwalled carbon nanotubes functionalized with poly (acrylic acid) (mMWNTs) and magnetic-activated carbon particles were subcutaneously injected in mice. The draining lymph nodes were harvested at different times post administration to examine the lymphatic distribution of these particles. The short-term accumulation and toxicity of mMWNTs in the major organs were studied.

- ✓ mMWNTs had the same properties of lymph node mapping as magnetic-activated carbon particles in mice independent of lymph node metastasis. The degree of black staining of lymph nodes and concentration of mMWNTs had a dose–response relationship. Aggregation of magnetic particles was found around the metastatic foci within the lymph nodes. Footpad injection of mMWNTs did not cause any obvious local or systemic toxicities, and no particle agglomerates were found in the major organs. Conclusion: The feasibility of targeting magnetic carbon nanotubes to lymph nodes was demonstrated and the results support further studies for their potential use in diagnosing and treating cancer.

- ✓

- ✓ ***Magnetic Micro-bubbles Magnetic Particle Imaging for Angiography***
- ✓ **Magnetic particle imaging** (**MPI**) is a tomographic imaging technique that measures the magnetic fields generated by magnetic particles in a tracer. Magnetic Particle Imaging has potential applications in medicine and material science. I developed the theory and scanners for X-space Magnetic Particle Imaging (MPI), a new medical imaging technique that will revolutionize diagnostic imaging. X-space MPI will enable real-time angiography without radiation or iodine, as well as cancer detection using dynamic contrast enhancement. X-space MPI theory describes how a combination of strong magnetic field gradients and time varying magnetic fields can produce an image

of the concentration of an iron oxide tracer in the body. The theory has been the foundation for my construction of three generations of X-space *MPI*scanners, the latest of which recently acquired our first animal images. *MPI* is the first whole-body imaging tech to see a radiation-free tracer w/ perfect contrast, giving doctors a powerful new diagnostic tool Heart disease is the leading cause of death in the US. *MPI* will save lives by giving doctors a way to assess cardiovascular health in real-time without the dangers of radiation and Iodine inherent to the clinically dominant X-ray techniques. *MPI* will also give scientists and health professionals a way to non-invasively study the body. *MPI* sees only an iron-oxide tracer and does not see tissue, and so *MPI* contrast is comparable to nuclear imaging. Therefore *MPI* could prove a radiation-free means to track tagged cells such as stem cells homing to an injury or monocytes seeking out an infection.

- ✓ Magnetic particle imaging (MPI) is an emerging modality that offers the potential for three-dimensional imaging with high sensitivity, high resolution and high imaging speed. The technique works by imaging the distribution of superparamagnetic nanoparticles injected into the body – achieved by measuring their response to an oscillating magnetic field.

- ✓ To image the nanoparticle distribution, a strong static magnetic gradient field is applied across the entire target. This selection field saturates the particles' magnetization everywhere besides a single field-free point (FFP). Drive coils then superimpose an oscillating magnetic field, and the nanoparticles' response is detected by a series of receive coils.

- ✓ As superparamagnetic nanoparticles exhibit a nonlinear response to an oscillating field, the detected signal contains higher-order harmonics that can be exploited for imaging. Only particles whose magnetic response is not suppressed by saturation, i.e. those in the direct vicinity of the FFP, will generate harmonics that contribute to the measured signal. Scanning the FFP through the sample thereby enables reconstruction of a full tomographic image of particle distribution.

- ✓ key component in the MPI process is the nanoparticle itself. While MPI resolution is intrinsically limited by the gradient strength, it is also dependent upon the size of the nanoparticle's magnetic core, and generally increases with core size. As well as being optimized in size, nanoparticles for use in MPI should have minimal variability in volume distribution, as well as a magnetic relaxation time that's fast enough to respond to the excitation field. With these constraints in mind, Ferguson and colleagues are developing new types of biocompatible iron-oxide (Fe_3O_4) nanoparticles.

- ✓ Microbubbles are tiny bubbles of gas (1-10μm in diameter) coated with a surfactant or polymer shell. When injected into the blood stream, microbubbles circulate around the body and dramatically enhance ultrasound images, as they are several thousand times more reflective than normal body tissue. They can also be used as delivery vehicles, as drugs or genes can be carried within a microbubble until the bubble is burst by ultrasound, releasing its cargo. Moreover, subjecting cells to low-intensity ultrasound in the presence of microbubbles creates temporary holes in cell membranes (a phenomenon known as sonoporation), enabling uptake of large molecules by cells.
- ✓ Researchers at UCL have developed microbubbles that have non-toxic magnetic nanoparticles incorporated into their shell. Instead of circulating freely, these magnetic

microbubbles have the potential to be targeted to an area of interest by the external application of a magnetic field. This bypasses the need to tailor-make microbubbles to specifically target different organs, and is more conducive to human therapy than the current method of targeting microbubbles by labelling them with monoclonal antibodies produced in animal cell cultures.

- ✓ Magnetic microbubbles may prove of significant value in both basic research and clinical settings.
- ✓ Potential applications in vitro include:
- ✓ -Efficient, non-viral transfection - the sonoporation effect of magnetic microbubbles on cells is enhanced when used in the presence of an applied magnetic field, improving transfection efficiency even with low doses of DNA
- ✓ -Delivery of siRNA into cells for gene knockdown
- ✓ -Labelling cells with fluorescent dye molecules or tagged antibodies for use in cell imaging
- ✓ Potential advantages to ultrasound imaging include:
- ✓ -Local concentration of microbubbles- this would increase signal strength from that region whilst reducing the administered dose
- ✓ -Manipulation of the flow of microbubbles - this would be useful in, for example, perfusion imaging, where the rate of flow of microbubbles into an organ is measured as an assessment of the organ's function. Such enhanced ultrasound imaging will be of benefit when investigating the pathology of disease states, for example metastases of the liver, as well as the characterisation of disease states, for example determining the

angiogenic phenotype of a tumour, in order to assess prognosis and potential response to available therapies.

- ✓ Other potential therapeutic applications include:
- ✓ -Drug or gene delivery to specific sites, minimising side effects and reducing the administered dose
- ✓ -Improved uptake of genetic material by cells as a result of sonoporation by localised microbubbles for use in gene therapy or therapeutic RNA inhibition
- ✓ -Non-invasive lysis of blood clots by localised sonoporation
- ✓ -Localised delivery of MRI contrast reagents, reducing side effects and the administered dose
- ✓ -Localising and intensifying cavitation activity in the target region during high intensity focused ultrasound (HIFU) surgery, thereby reducing the ultrasound intensities and treatment times required
- ✓
- ✓
- ✓